EBERHARD KARLS
UNIVERSITÄT
TÜBINGEN

What did we learn from the detection of gravitational waves?

Kostas Kokkotas

Theoretical Astrophysics

Eberhard Karls University of Tübingen

The «Beginning» of an new Era

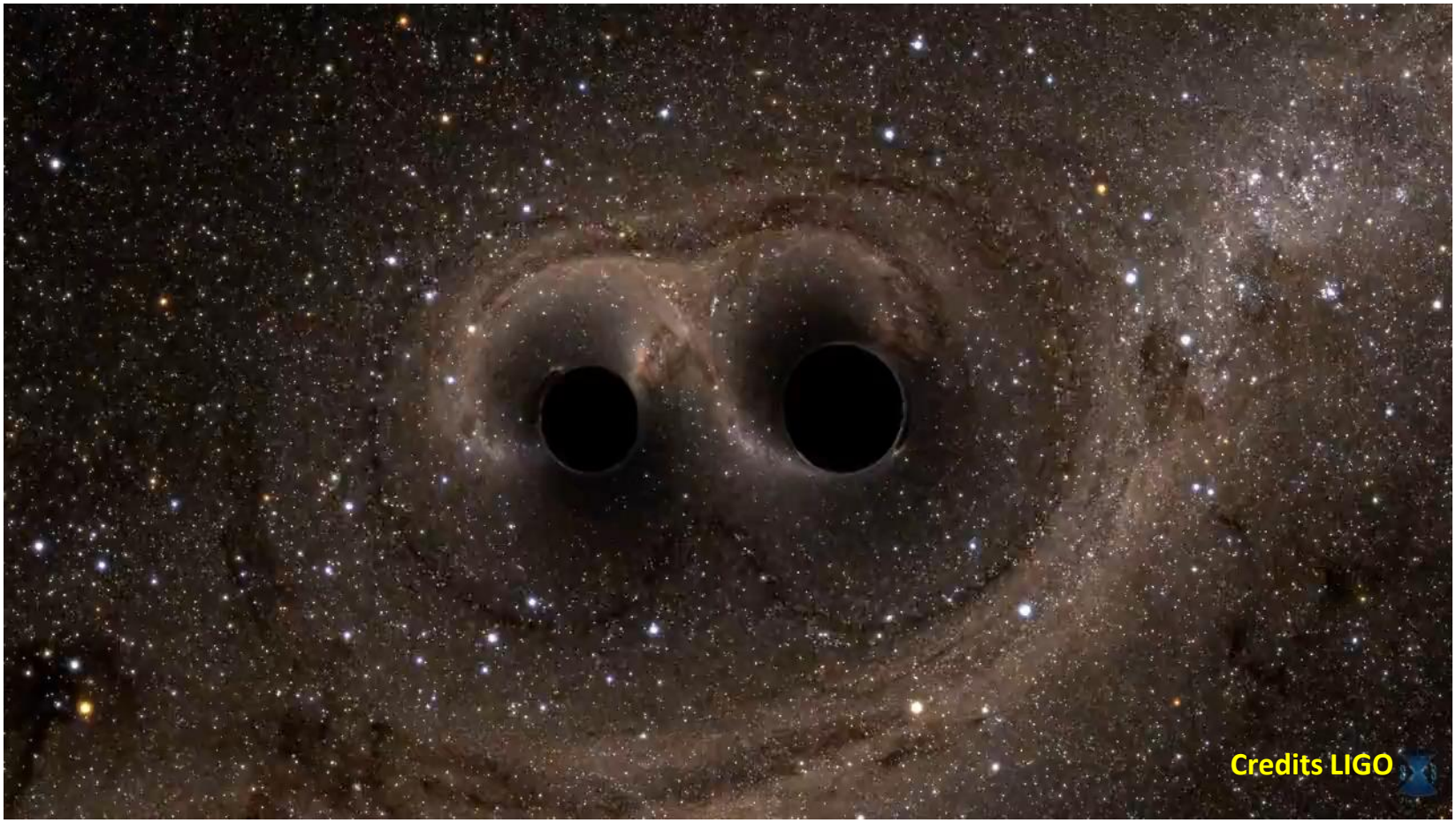

The «SOUND» of Vacuum

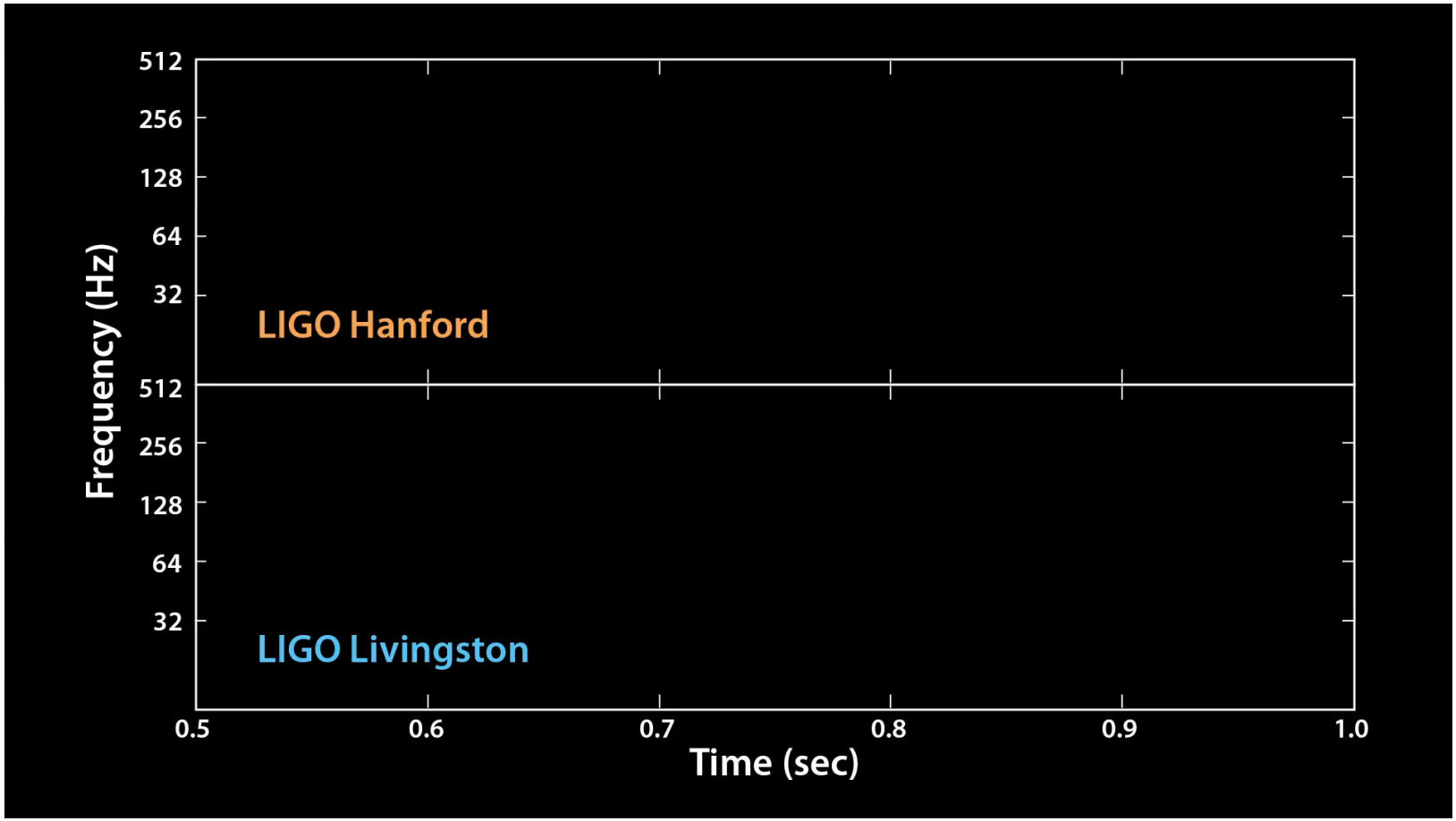

What did they Observe?

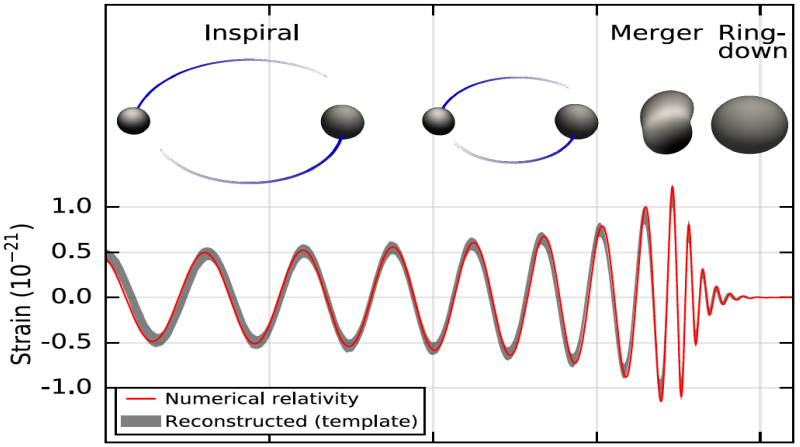

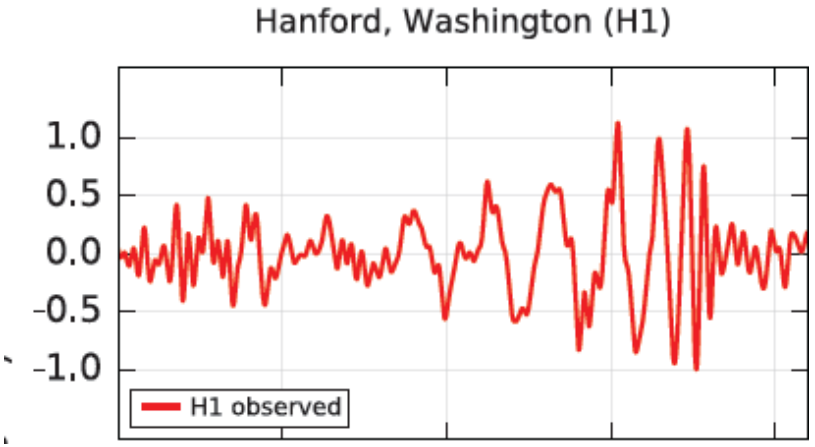

M_1	: 36^{+5}_{-4} $M_\odot$
M_2	: 29^{+4}_{-4} $M_\odot$
S/N	: ~24
Spin	: 0.67
Final Mass	: 62^{+4}_{-4} $M_\odot$
Distance	: 410^{+160}_{-180} Mpc
	~1.3 x 10^9 light years
Redshift	: z~$0.09^{+0.03}_{-0.04}$

GW150914

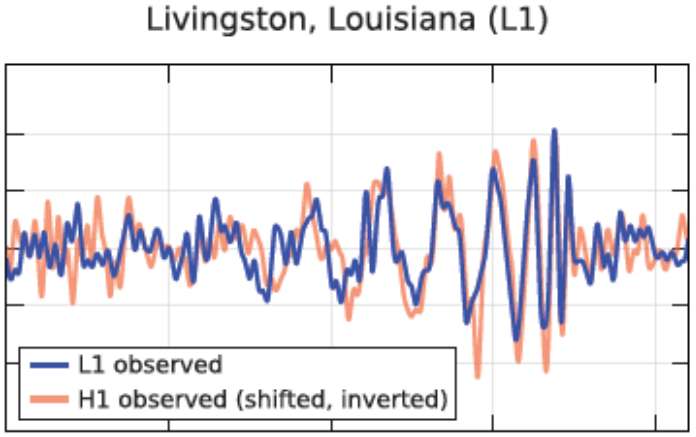

BORING: Binary BH mergers again and again!!

	SNR	M_1 ($M_\odot$)	M_2 ($M_\odot$)	D (Mpc)	Spin (final)
GW150914	23.7	36	29	440	68%
LVT151012	9.7	23	13	1000	66%
GW151226	13	14.2	7.5	440	74%
GW170114	10	31.2	19.4	880	64%
GW170608	13	12	7	340	69%
GW170814	(18)	30.5	25.3	540	70%

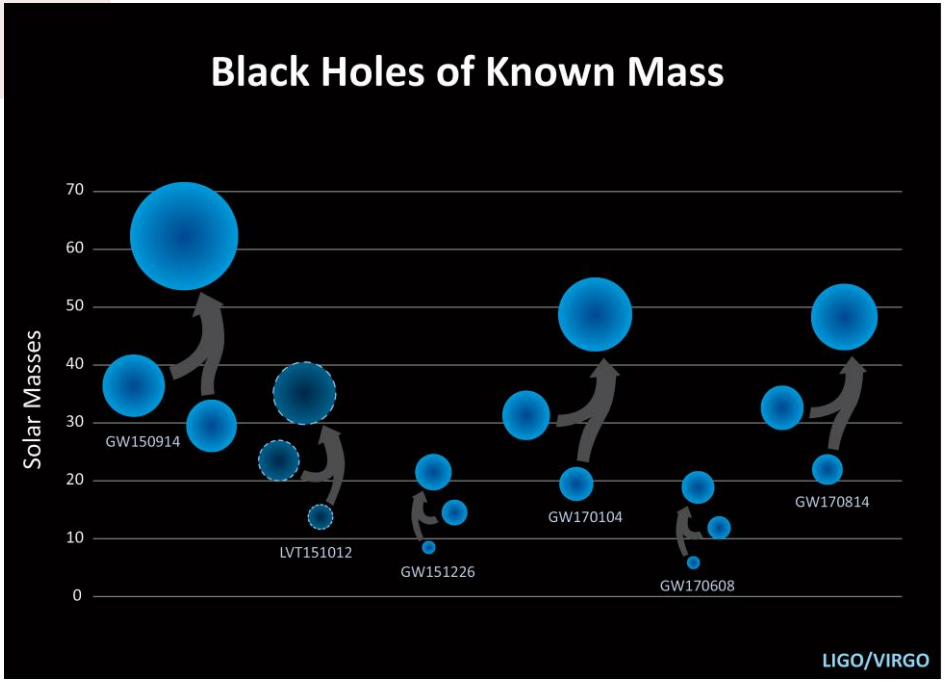

The Catalog of GW Events

O1 & O2 Runs

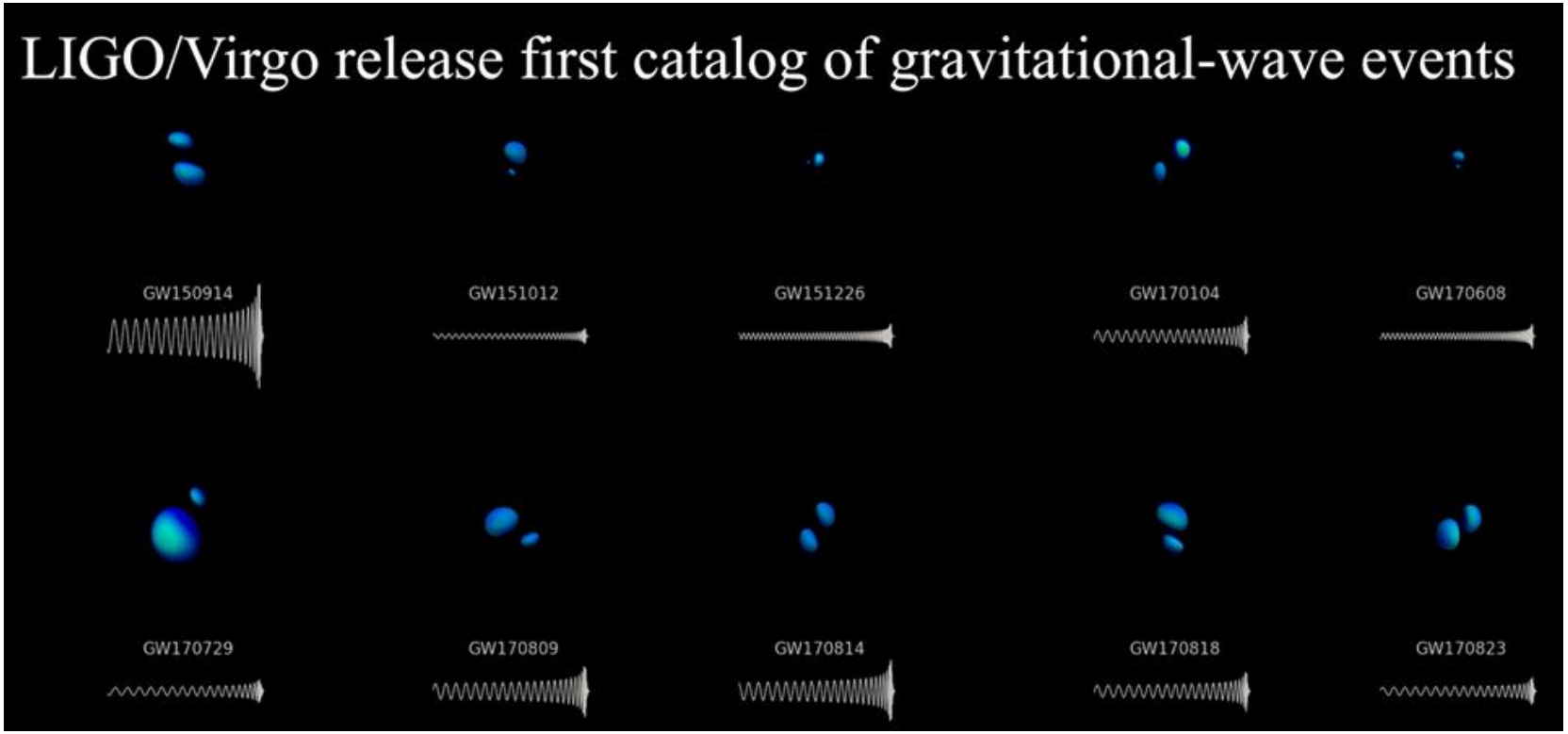

The Catalog of GW Events

1st & 2nd Run

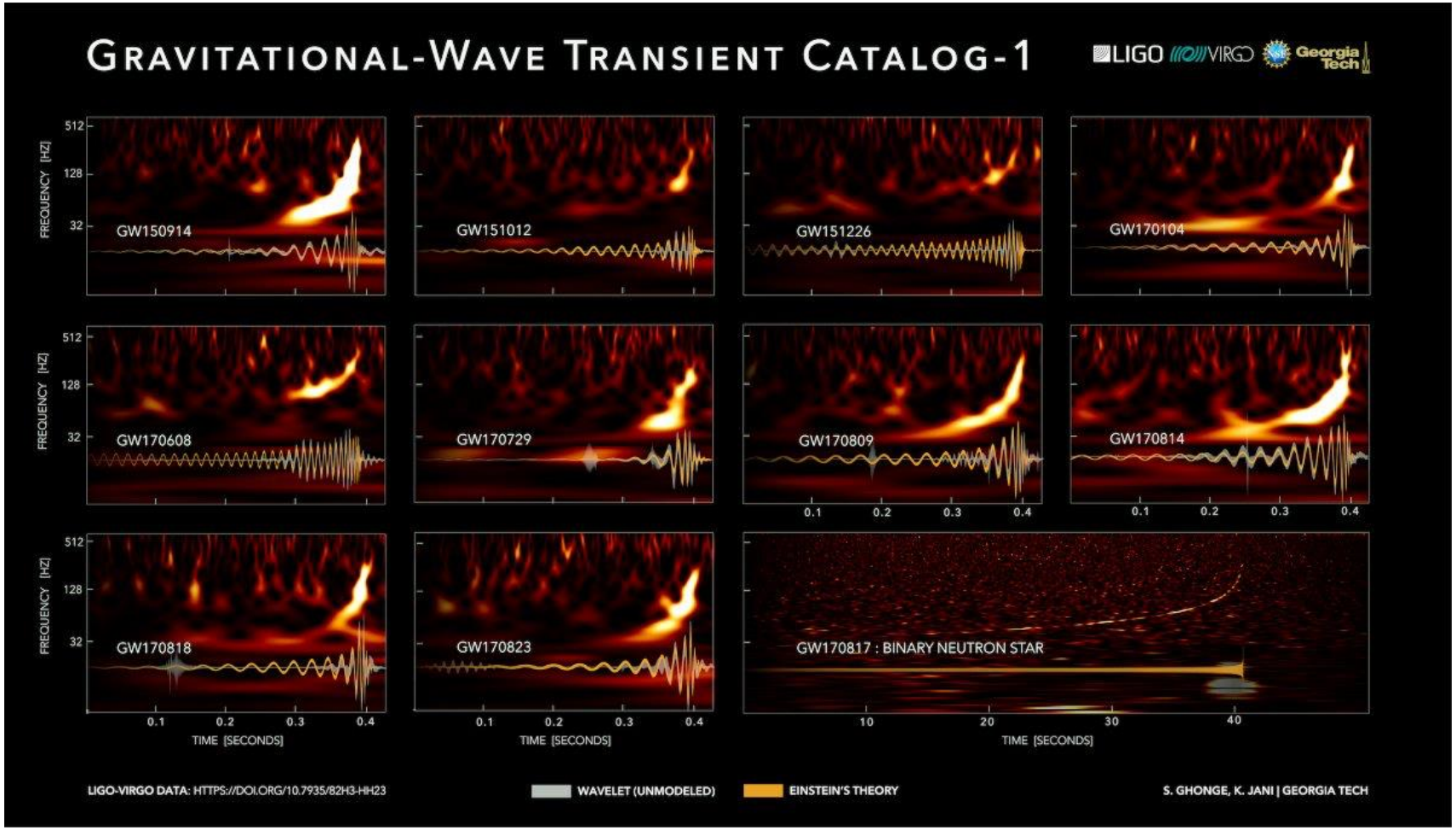

Positioning the Sources (GW170814)

1160 deg²

60 deg²

In the direction of Eridanus constellation

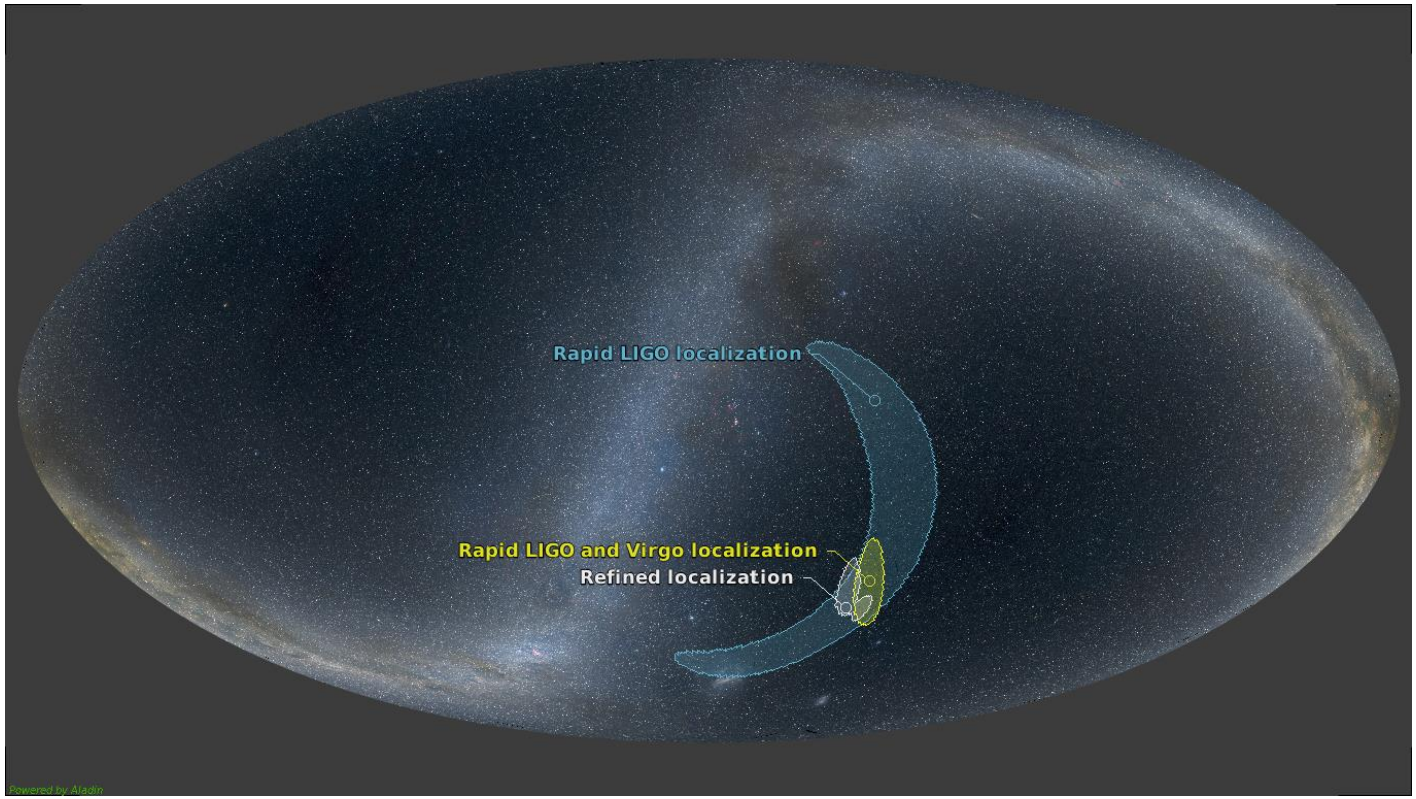

Prepare for the Unexpected
GW170817

Neutron Star Mergers
GW170817

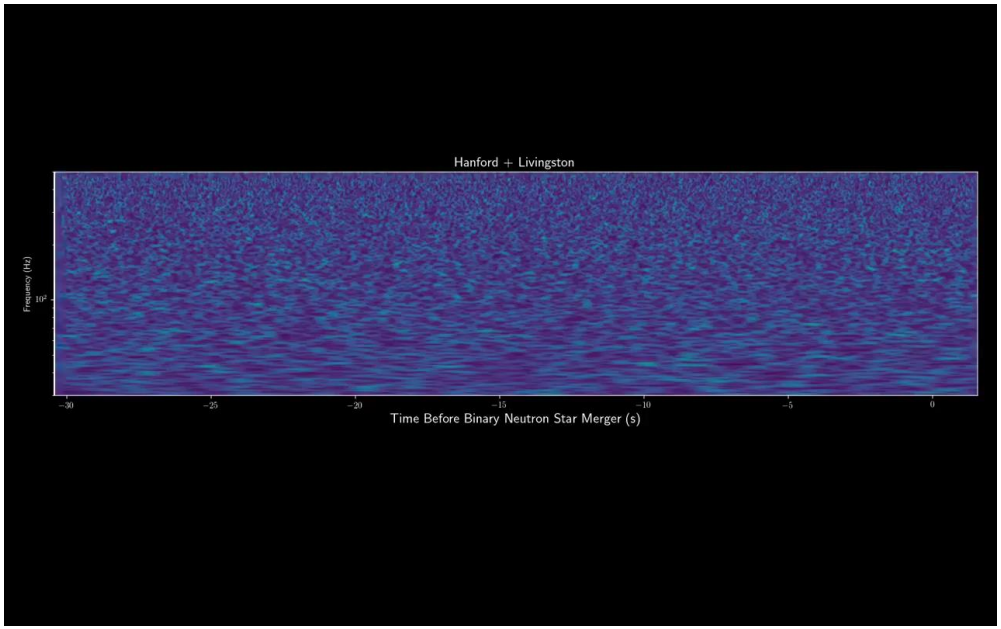

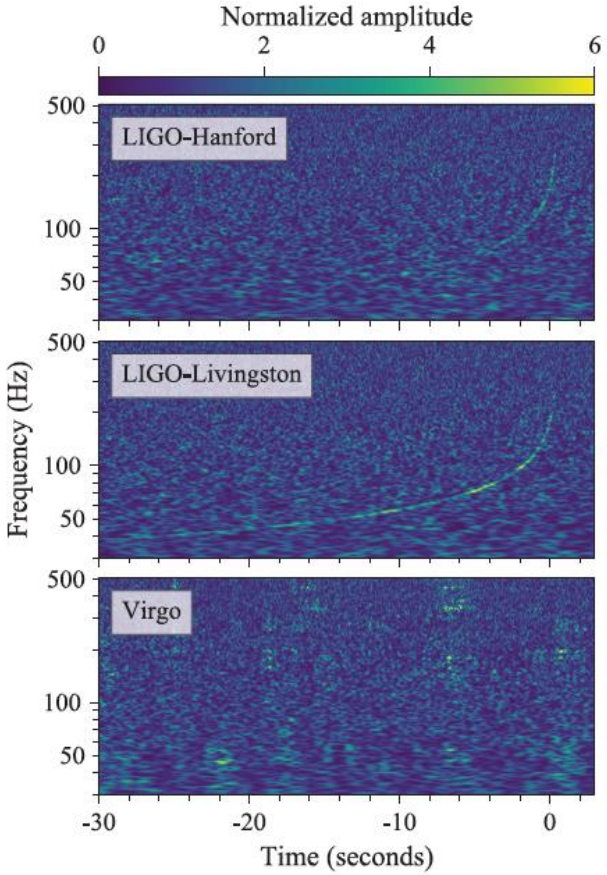

S/N	~ 32.4
Duration	~ 100 sec
M_1	~1.36-1.60 $M_\odot$
M_2	~1.17-1.36 $M_\odot$
Radiated energy	~0.025 $M_\odot c^2$
Luminosity dist.	~ 40 Mpc

Dimensionless tidal deformability $\Lambda(1.4\ M_\odot) < 800$

Neutron Star Mergers
constraining the speed of gravity

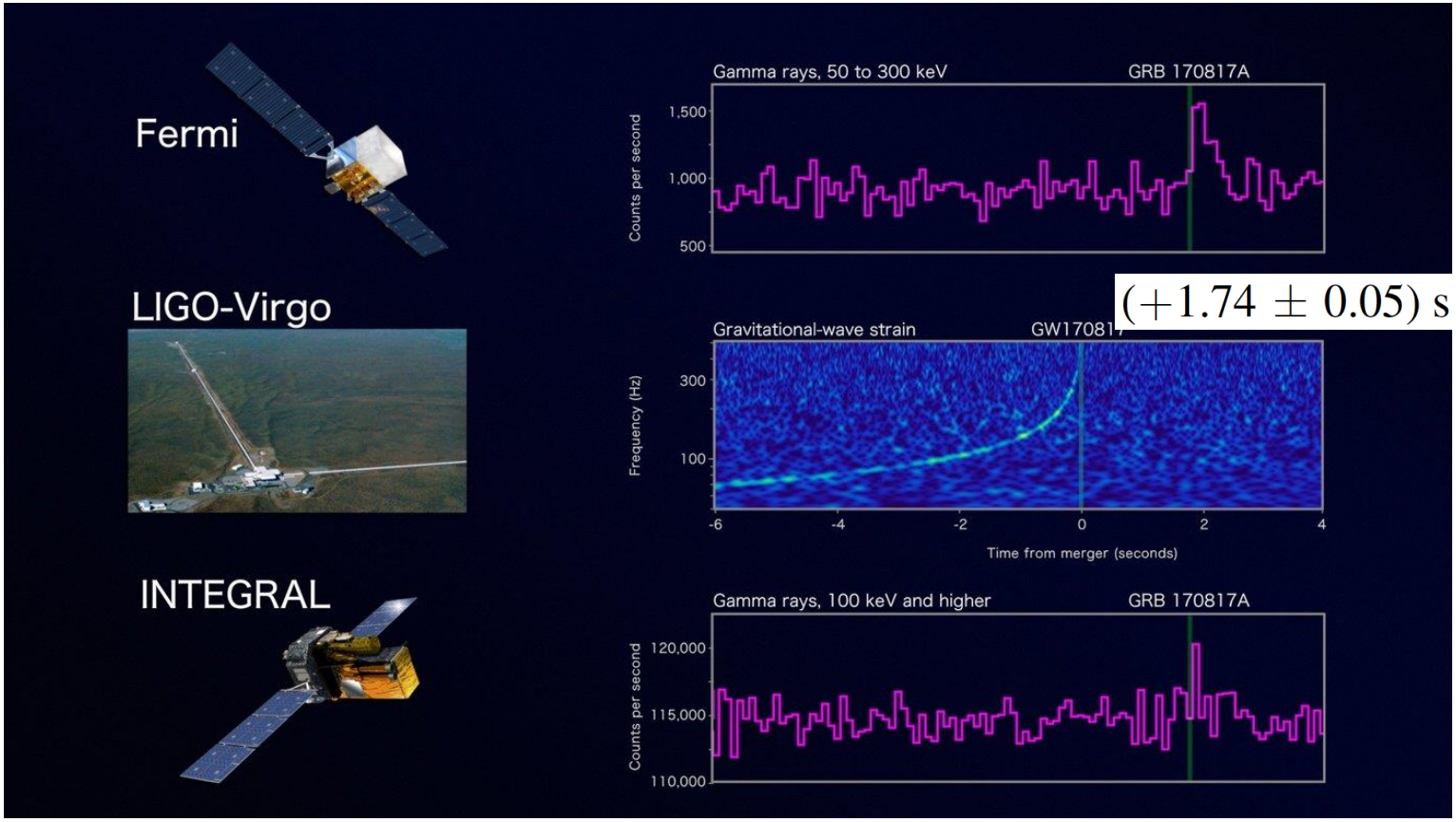

Neutron Star Mergers
constraining the speed of gravity

Speed of Gravity

Assuming a small difference in travel time Δt between photons and GWs, and the known travel distance D, the functional speed difference will be

$$Dv = v_{GW} - v_{EM}$$

The resulting (conservative) constraint

$$-3 \times 10^{-15} \leqslant \frac{\Delta v}{v_{EM}} \leqslant +7 \times 10^{-16}$$

Alternative theories predicting massive gravitons were "brutally and pitilessly murdered" (TeVeS, Galileon theories, etc)

Test of the Equivalence Principle

By probing whether EM radiation and GWs are affected by background gravitational potentials in the same way is a test of the equivalence principle.

The Shapiro delay for massless particles can be measured as:

$$\delta t_S = -\frac{1+\gamma}{c^3}\int_{r_e}^{r_o} U(\boldsymbol{r}(l))dl$$

where **γ** parametrizes a deviation from Einstein-Maxwell theory (where $\gamma_{GW} = \gamma_{EM} = 1$). The limits are:

$$-2.6 \times 10^{-7} \leqslant \gamma_{GW} - \gamma_{EM} \leqslant 1.2 \times 10^{-6}.$$

The best absolute bound from Cassini spacecraft is: $\gamma_{EM} - 1 = (2.1 \pm 2.3) \times 10^{-5}$

Neutron Star Mergers

GW - EM Observatories

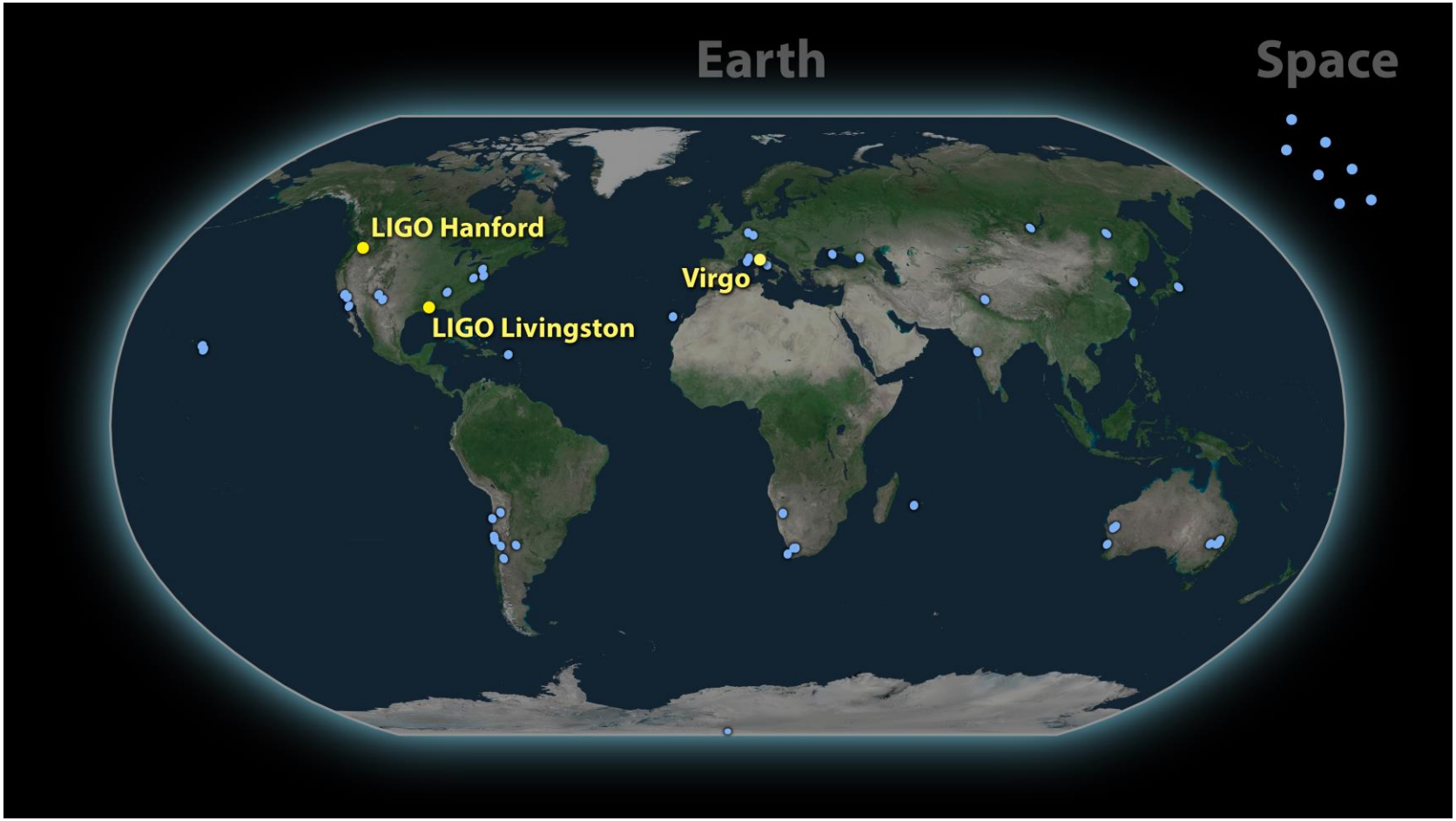

Neutron Star Mergers
Sequence of Events

12:41:04 UTC	A **Gravitational Wave** from binary NS merger is detected
+2 sec	A **Short Gamma ray** burst is detected
	GW + EM from the same source provide compelling evidence that **GWs travel with the speed of light**
	The two events allow for the **measure of the expansion rate of the Universe**
	Kilonova: neutron star mergers responsible for the production of heavy elements in the universe.
+10 h **52** min	A new bright source of **optical light** is detected in a galaxy called NGC 4993 (constellation of Hydra)
+11 h **36** min	**Infrared emission** observed
+15 h	**Bright ultraviolet** emission detected
+9 days	**X-ray** emission detected
+16 days	**Radio** emission detected

Neutron Star Mergers

Alchemy or Heavy Element Production

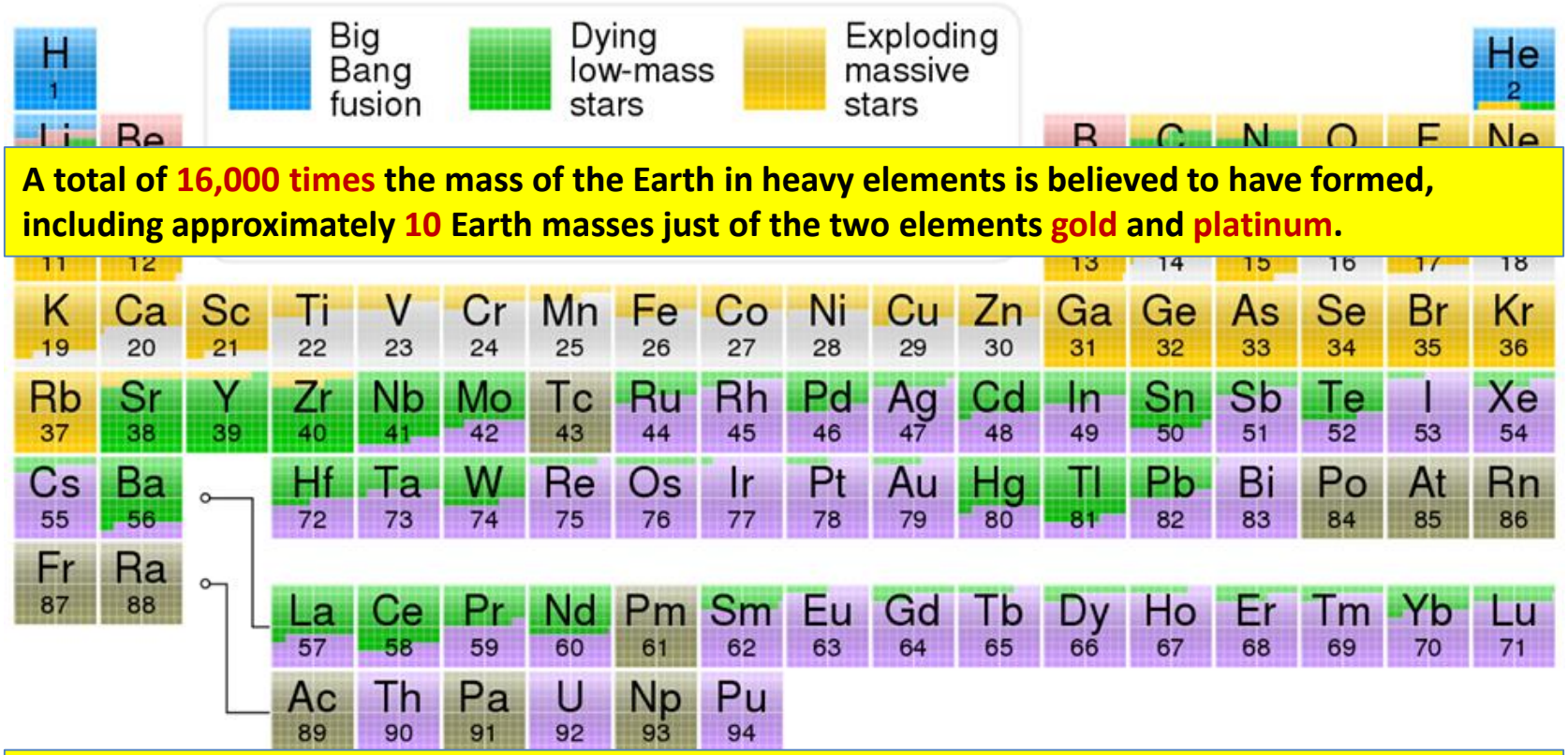

A total of 16,000 times the mass of the Earth in heavy elements is believed to have formed, including approximately 10 Earth masses just of the two elements gold and platinum.

Light emitted after a neutron star collision showed signs of heavy elements present in the aftermath, confirming that certain elements (purple) are produced in such mergers

Masses of the Detected BHs and NSs

1st & 2nd Run

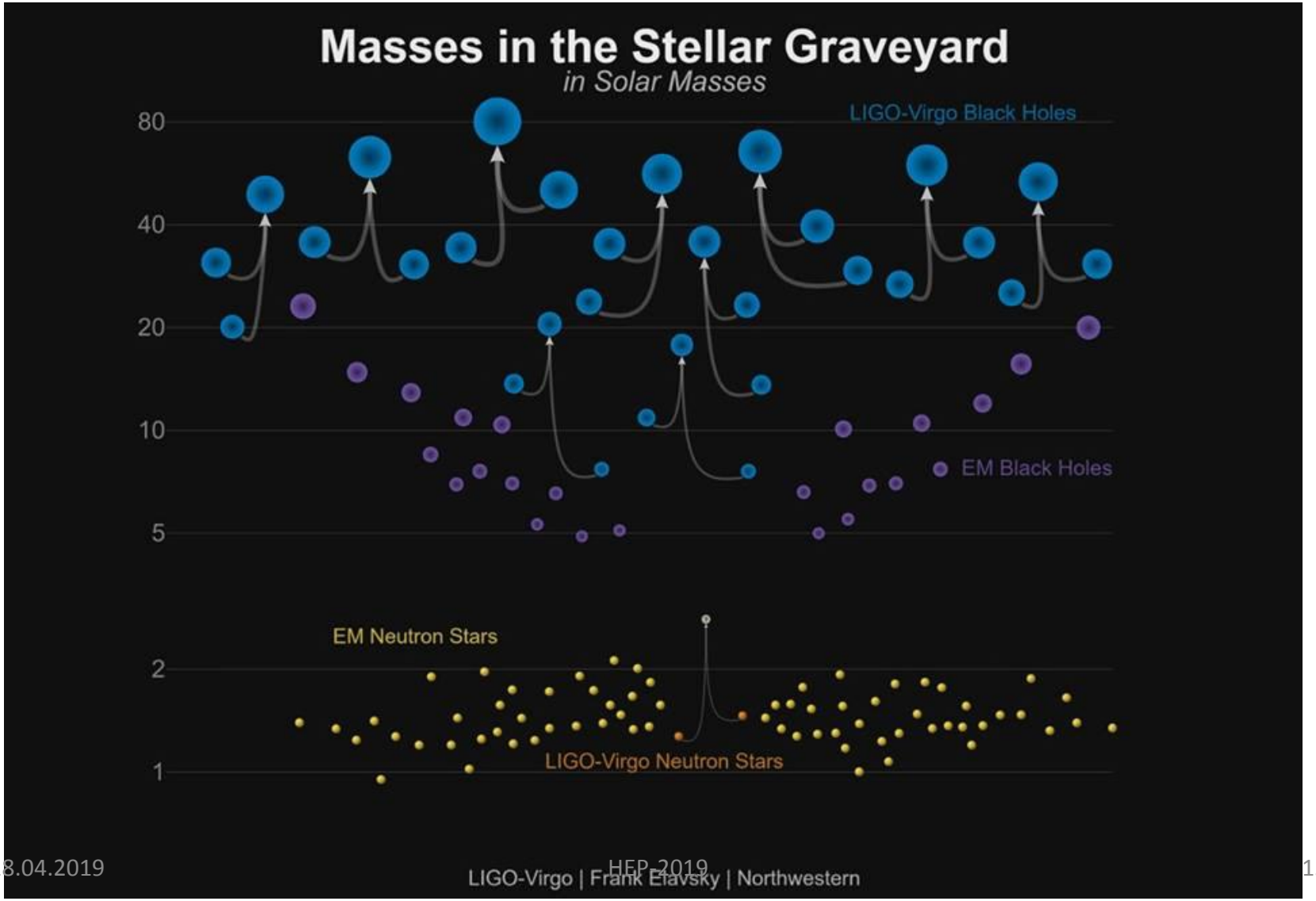

Masses of the Detected BHs and NSs

1st & 2nd Run

Event	$m_1/M_\odot$	$m_2/M_\odot$	$\mathcal{M}/M_\odot$	$\chi_{\rm eff}$	$M_{\rm f}/M_\odot$	$a_{\rm f}$	$E_{\rm rad}/(M_\odot c^2)$	$\ell_{\rm peak}/({\rm erg\,s^{-1}})$	$d_L/{\rm Mpc}$	z	$\Delta\Omega/{\rm deg}^2$
GW150914	$35.6^{+4.8}_{-3.0}$	$30.6^{+3.0}_{-4.4}$	$28.6^{+1.6}_{-1.5}$	$-0.01^{+0.12}_{-0.13}$	$63.1^{+3.3}_{-3.0}$	$0.69^{+0.05}_{-0.04}$	$3.1^{+0.4}_{-0.4}$	$3.6^{+0.4}_{-0.4}\times10^{56}$	430^{+150}_{-170}	$0.09^{+0.03}_{-0.03}$	179
GW151012	$23.3^{+14.0}_{-5.5}$	$13.6^{+4.1}_{-4.8}$	$15.2^{+2.0}_{-1.1}$	$0.04^{+0.28}_{-0.19}$	$35.7^{+9.9}_{-3.8}$	$0.67^{+0.13}_{-0.11}$	$1.5^{+0.5}_{-0.5}$	$3.2^{+0.8}_{-1.7}\times10^{56}$	1060^{+540}_{-480}	$0.21^{+0.09}_{-0.09}$	1555
GW151226	$13.7^{+8.8}_{-3.2}$	$7.7^{+2.2}_{-2.6}$	$8.9^{+0.3}_{-0.3}$	$0.18^{+0.20}_{-0.12}$	$20.5^{+6.4}_{-1.5}$	$0.74^{+0.07}_{-0.05}$	$1.0^{+0.1}_{-0.2}$	$3.4^{+0.7}_{-1.7}\times10^{56}$	440^{+180}_{-190}	$0.09^{+0.04}_{-0.04}$	1033
GW170104	$31.0^{+7.2}_{-5.6}$	$20.1^{+4.9}_{-4.5}$	$21.5^{+2.1}_{-1.7}$	$-0.04^{+0.17}_{-0.20}$	$49.1^{+5.2}_{-3.9}$	$0.66^{+0.08}_{-0.10}$	$2.2^{+0.5}_{-0.5}$	$3.3^{+0.6}_{-0.9}\times10^{56}$	960^{+430}_{-410}	$0.19^{+0.07}_{-0.08}$	924
GW170608	$10.9^{+5.3}_{-1.7}$	$7.6^{+1.3}_{-2.1}$	$7.9^{+0.2}_{-0.2}$	$0.03^{+0.19}_{-0.07}$	$17.8^{+3.2}_{-0.7}$	$0.69^{+0.04}_{-0.04}$	$0.9^{+0.0}_{-0.1}$	$3.5^{+0.4}_{-1.3}\times10^{56}$	320^{+120}_{-110}	$0.07^{+0.02}_{-0.02}$	396
GW170729	$50.6^{+16.6}_{-10.2}$	$34.3^{+9.1}_{-10.1}$	$35.7^{+6.5}_{-4.7}$	$0.36^{+0.21}_{-0.25}$	$80.3^{+14.6}_{-10.2}$	$0.81^{+0.07}_{-0.13}$	$4.8^{+1.7}_{-1.7}$	$4.2^{+0.9}_{-1.5}\times10^{56}$	2750^{+1350}_{-1320}	$0.48^{+0.19}_{-0.20}$	1033
GW170809	$35.2^{+8.3}_{-6.0}$	$23.8^{+5.2}_{-5.1}$	$25.0^{+2.1}_{-1.6}$	$0.07^{+0.16}_{-0.16}$	$56.4^{+5.2}_{-3.7}$	$0.70^{+0.08}_{-0.09}$	$2.7^{+0.6}_{-0.6}$	$3.5^{+0.6}_{-0.9}\times10^{56}$	990^{+320}_{-380}	$0.20^{+0.05}_{-0.07}$	340
GW170814	$30.7^{+5.7}_{-3.0}$	$25.3^{+2.9}_{-4.1}$	$24.2^{+1.4}_{-1.1}$	$0.07^{+0.12}_{-0.11}$	$53.4^{+3.2}_{-2.4}$	$0.72^{+0.07}_{-0.05}$	$2.7^{+0.4}_{-0.3}$	$3.7^{+0.4}_{-0.5}\times10^{56}$	580^{+160}_{-210}	$0.12^{+0.03}_{-0.04}$	87
GW170817	$1.46^{+0.12}_{-0.10}$	$1.27^{+0.09}_{-0.09}$	$1.186^{+0.001}_{-0.001}$	$0.00^{+0.02}_{-0.01}$	≤ 2.8	≤ 0.89	≥ 0.04	$\geq 0.1\times10^{56}$	40^{+10}_{-10}	$0.01^{+0.00}_{-0.00}$	16
GW170818	$35.5^{+7.5}_{-4.7}$	$26.8^{+4.3}_{-5.2}$	$26.7^{+2.1}_{-1.7}$	$-0.09^{+0.18}_{-0.21}$	$59.8^{+4.8}_{-3.8}$	$0.67^{+0.07}_{-0.08}$	$2.7^{+0.5}_{-0.5}$	$3.4^{+0.5}_{-0.7}\times10^{56}$	1020^{+430}_{-360}	$0.20^{+0.07}_{-0.07}$	39
GW170823	$39.6^{+10.0}_{-6.6}$	$29.4^{+6.3}_{-7.1}$	$29.3^{+4.2}_{-3.2}$	$0.08^{+0.20}_{-0.22}$	$65.6^{+9.4}_{-6.6}$	$0.71^{+0.08}_{-0.10}$	$3.3^{+0.9}_{-0.8}$	$3.6^{+0.6}_{-0.9}\times10^{56}$	1850^{+840}_{-840}	$0.34^{+0.13}_{-0.14}$	1651

LIGO 1811.12907

Sky maps of the detected BHs and NSs

1st & 2nd Run

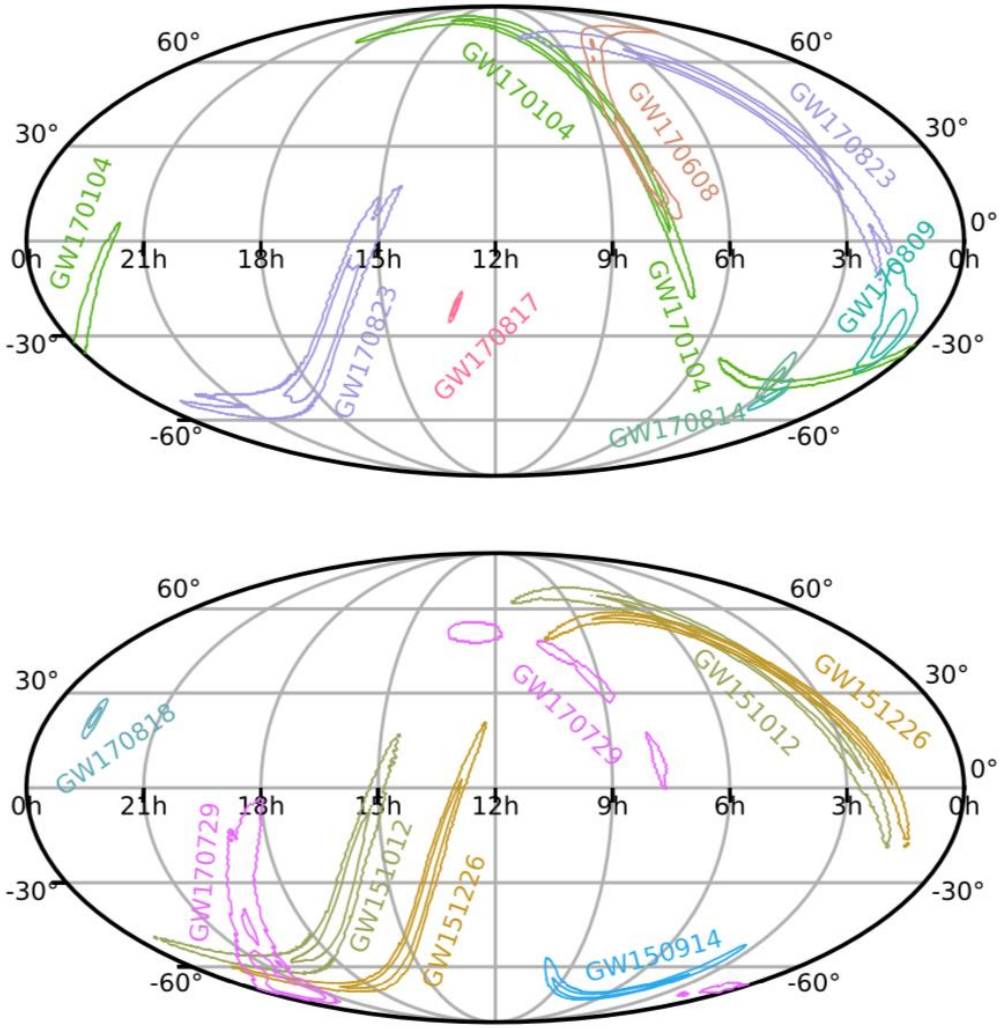

LIGO: 1811.12907

Binary BH Mergers vs Pulsars

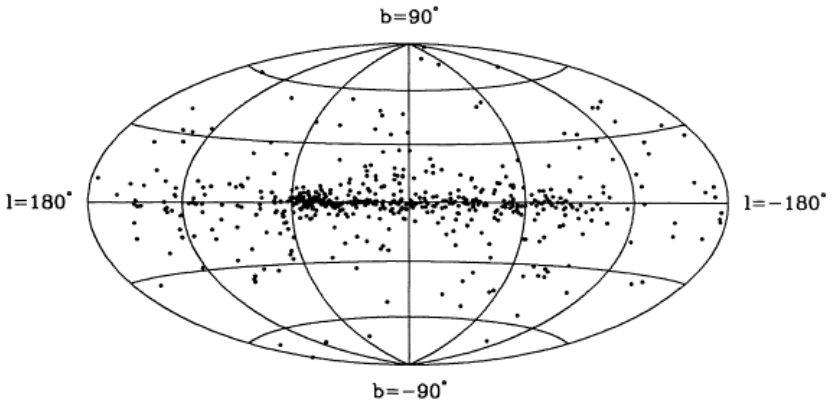

FIG. 1.—Distribution of 558 pulsars in Galactic coordinates, using the Hammer-Aitoff equal-area projection. The Galactic center is in the middle of the figure, and longitude increases toward the left.

- **16** years after the discovery of the 1st pulsar we observed **558** pulsars
- **52** years later **~2600+** new pulsars

  an easy bet…
- In **16** years after the 1st GW detection we should "see" **at least 10 times more Binary BH mergers!!**

TABLE 2
PULSAR PROPER MOTIONS

PSR J	PSR B	μ_α (mas yr^{-1})	±	μ_δ (mas yr^{-1})	±	Epoch (MJD)	Ref.
0139+5814	0136+57	−11	5	−19	5	46573	81
0151−0635	0148−06	15	47	−30	34	46901	81
0152−1637	0149−16	−10	50	−150	50	46573	57
0206−4028	0203−40	−10	25	75	35	46902	185
0255−5304	0254−53	0	20	70	15	46916	185
0304+1932	0301+19	6	7	−37	4	46058	116
0323+3944	0320+39	16	6	−30	5	46573	81
0332+5434	0329+54	17	1	−13	1	40105	81
0358+5413	0355+54	5	4	6	3	46573	116
0450−1248	0447−12	0	20	−3	18	46573	81
0454+5543	0450+55	52	6	−17	2	46460	81
0452−1759	0450−18	19	8	35	18	46573	57
0502+4654	0458+46	−8	3	8	5	46460	81
0525+1115	0523+11	30	7	−4	5	46058	81
0528+2200	0525+21	−20	19	7	9	41994	81
0534+2200	0531+21	−12	3	5	4	40675	226
0543+2329	0540+23	19	7	12	8	47555	81
0601−0527	0559−05	18	8	−16	7	44240	81
0614+22	0611+22	−4	5	−3	7		81
0629+2415	0626+24	−7	12	2	12	47555	81
0630−2834	0628−28	−5	18	−17	26	40585	57
0653+8051	0643+80	19	3	−1	3	46460	81
0700+6418	0655+64	1	35	−14	29	46000	81
0659+1414	0656+14	−71	12	32	12	47552	200
0738−4042	0736−40	−56	9	46	8	41331	51
0742−2822	0740−28	−29.0	9	−0.1	4	46573	15
0754+32	0751+32	−4	5	7	3	44240	81
0814+7429	0809+74	15	7	−49	6	42077	116
0820−1350	0818−13	9	10	−31	7	46573	81
0823+0159	0820+02	5	11	−1	8	44546	81
0826+2637	0823+26	61	3	−90	2	40264	116
0835−4510	0833−45	−48	2	35	1	43180	15
0837+0610	0834+06	2	5	51	3	46058	116
0908−1739	0906−17	27	11	−40	11	44240	81
0922+0638	0919+06	13	29	64	37	46573	81
0943+1631	0940+16	23	16	9	11	47555	81
0944−1354	0942−13	−1	32	−22	14	44240	81
0946+09	0943+10	−38	19	−21	12		116
0953+0755	0950+08	15	8	31	5	46058	116
1115+5030	1112+50	22	3	−51	3	44240	81
1136+1551	1133+16	−102	5	357	3	42364	116
1239+2453	1237+25	−106	4	42	3	46058	116
1321+8323	1322+83	−53	20	13	7	46460	81
1430−6623	1426−66	−31	5	−21	3	46916	15
1453−6413	1449−64	−16	1	−21.3	8	46917	15
1456−6843	1451−68	−39.5	4	−12.3	3	43560	15
1509+5531	1508+55	−73	4	−68	3	42058	116
1543−0620	1540−06	32	35	−56	20	46573	57
1543+0929	1541+09	−12	4	3	3	42304	116
1559−4438	1556−44	−11	17	20	50	43570	57
1604−4909	1600−49	−30	7	−1	3	43837	15
1607−0032	1604−00	−1	14	−7	9	42307	116
1645−0317	1642−03	41	17	−25	11	40414	116
1709−1640	1706−16	75	20	147	50	41331	57
1720−0212	1718−02	26	9	−13	6	44240	81
1752−2806	1749−28	−5	17	8	15	40352	57
1807−0847	1804−08	8	15	4	20	46573	57
1820−0427	1818−04	3	3	27	2	40614	76
1823+0550	1821+05	5	11	−2	4	44240	81
1825−0935	1822−09	10	19	−23	19	46956	57
1840+5640	1839+56	−30	4	−21	2		81
1844+1454	1842+14	−9	10	45	6	44240	81
1857+0943	1855+09	−2.92	12	−5.32	19	47526	178
1900−2600	1857−26	−22	10	−44	7	46573	57
1907+4002	1905+39	11	4	11	1	44240	81
1913−0440	1911−04	7	13	−5	9	41902	81
1915+1606	1913+16	−2.9	9	0.7	8	45888	193
1919+0021	1917+00	−2	30	−1	10	42426	81
1921+2153	1919+21	11	14	2	15	42084	57
1932+1059	1929+10	99	6	39	4	46917	52

Main Sources for LIGO/Virgo

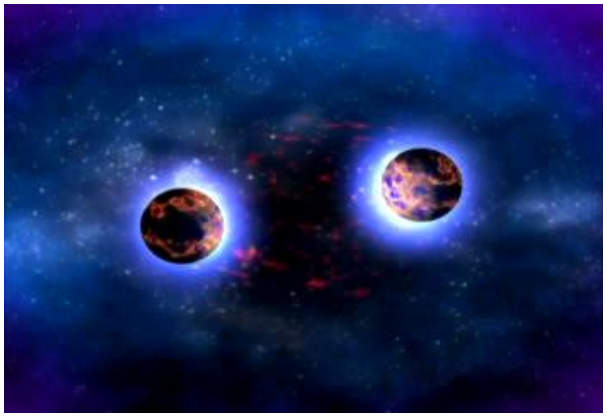

BH and NS Binaries

Supernovae, BH/NS formation

$$L_{GW} \sim \left(\frac{M}{R}\right)^5$$

$$h \sim e \cdot \left(\frac{M}{r}\right) \cdot \left(\frac{M}{R}\right)$$

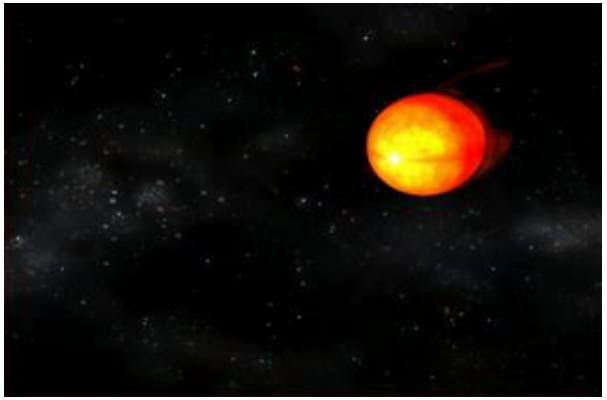

Spinning neutron stars in X-ray binaries

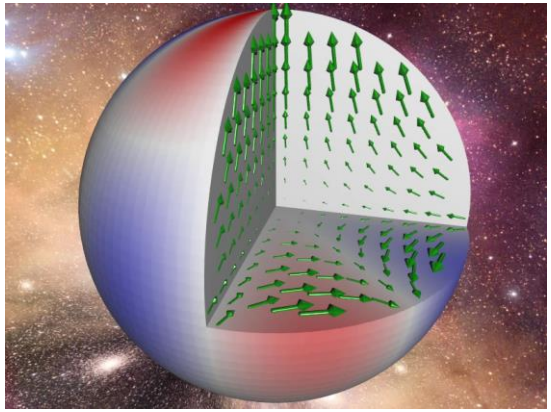

Neutron Stars:
Instabilities, Deformations

BLACK HOLES:	M/R=0.5
NEUTRON STARS:	M/R~0.2
WHITE DWRFS:	M/R~10^{-4}

The "Operational" Detectors for O3

LIGO (Livingston) : USA (4km)

$$\frac{D\ell}{\ell} = h$$

LIGO (Hanford) : USA (4km)

Virgo (Pisa) : Italy – France (3km)

- The O3 phase will last 12 months
- Sensitivity improved by about 40%

KAGRA:
Large-scale Cryogenic GW Telescope (Japan)

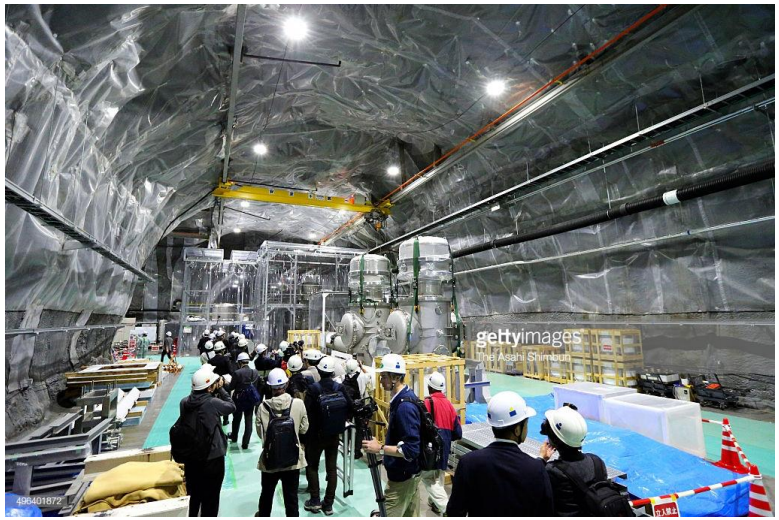

- KAGRA consists of a modified Michelson interferometer with two 3-km long arms, located in the ground under Kamioka mine.
- The mirrors are cooled down to cryogenic temperature of -250 Celsius degree (20 Kelvin). Sapphire is chosen for the material of the mirror.

Will join in early 2020

INDIGO (India-USA) : Similar to existing LIGOs

Binary BH Mergers : Fresh Detections

2019-04-08 18:18:23 UTC

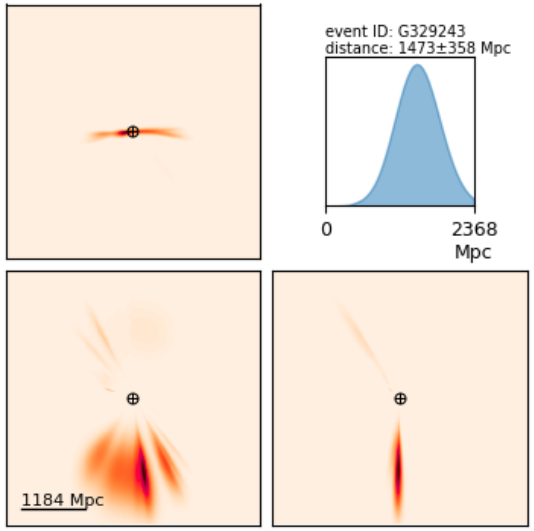

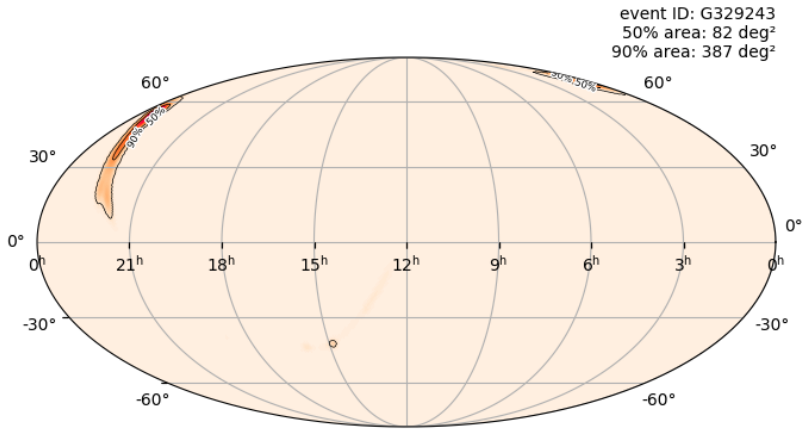

2019-04-12 07:28:32 GMT

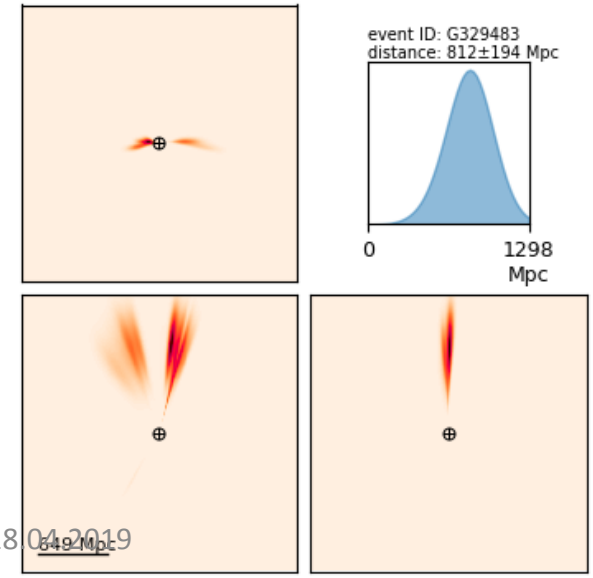

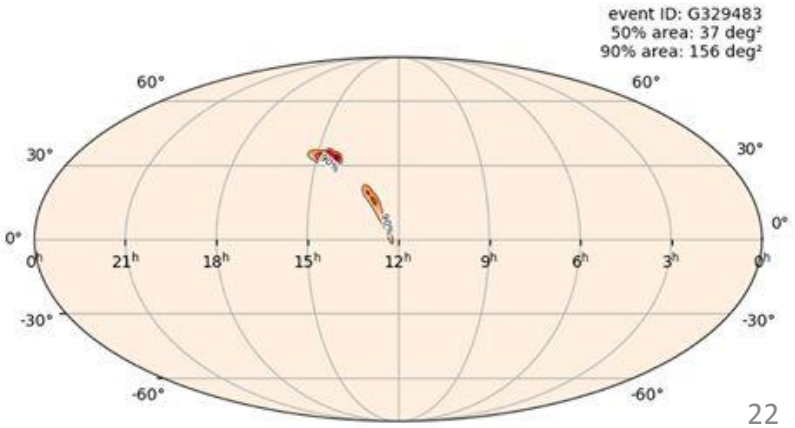

Expected Event Rates: Obs. Run 3 (O3)

A rough estimation:

— **several** black hole mergers **per month** should be seen by the detectors **(9.7-101 Gpc^{-3}/y)**
— and up to **one** neutron star merger **per month** as well **(110-3840 Gpc^{-3}/y)**
— comparable number of NS-BH events **(< 610 Gpc^{-3}/y)**

One **important measurement is the rate** at which these mergers occur in the universe, because by knowing this rate should yield a wealth of information — **about how black holes are formed**,
— how they find themselves in binary systems and
— how they gradually move close enough together to merge.

BH - BH

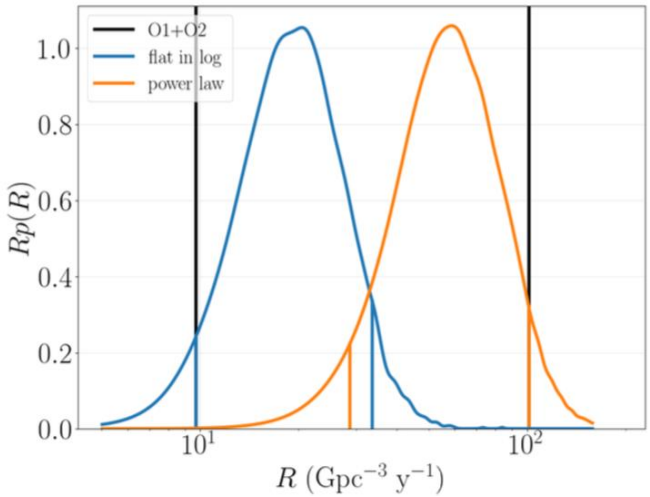

NS - NS

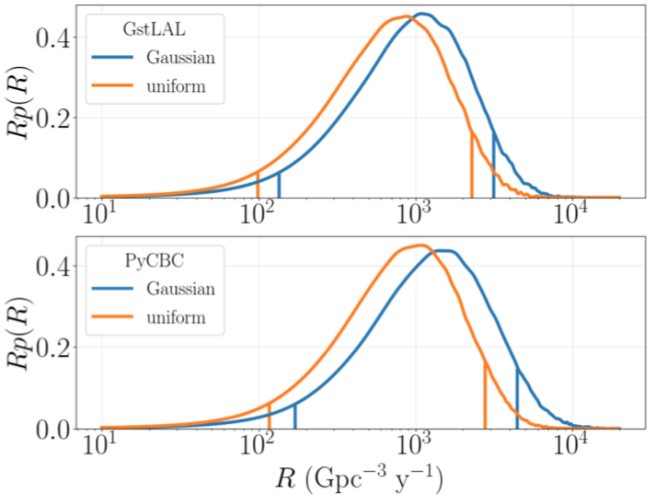

Einstein Telescope (2030+)

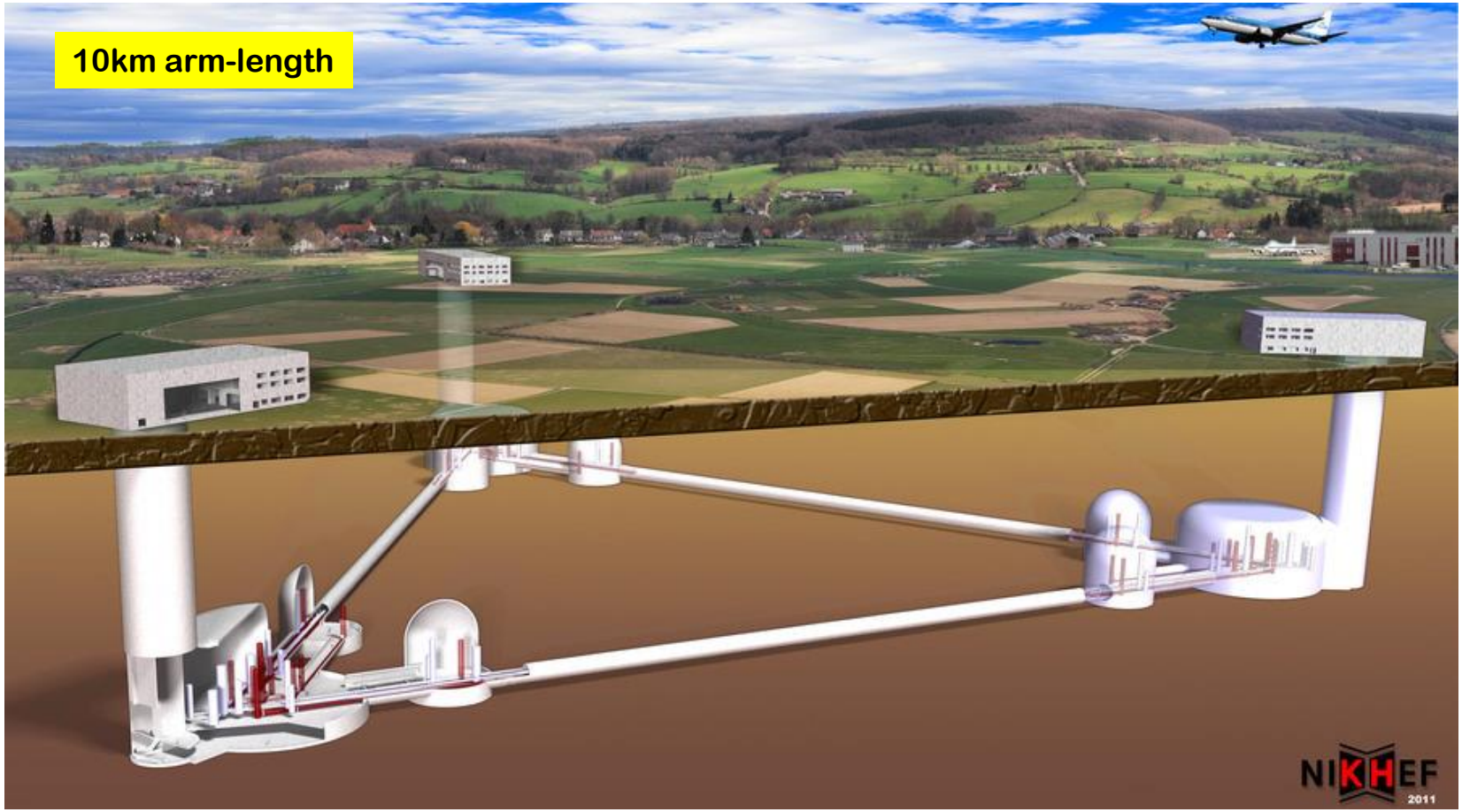

Netherlands, Germany, Poland, Russia, UK
Italy, France, Hungary

Cosmic Explorer (2030+)

A **40 km long detector**, 10 times longer than Adv. LIGO, is well suited to detecting signals:
-- From **binary NS systems** and **core-collapse supernovae** up to **4 kHz in frequency**.
-- This length also provides sensitivity sufficient to detect **binary black holes from anywhere in the Universe (up to redshift of roughly 100).**

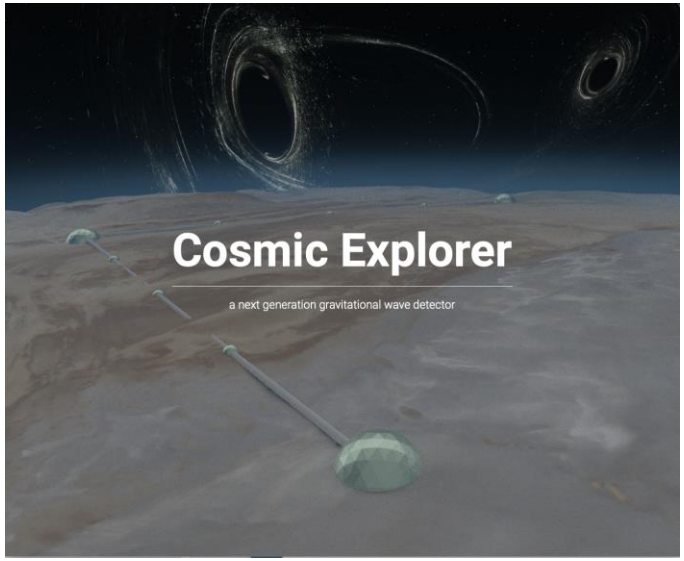

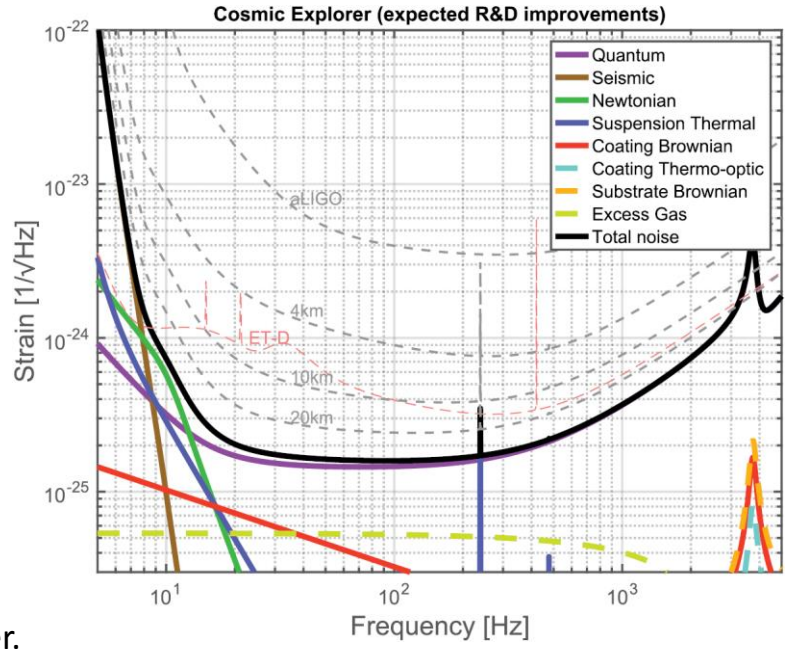

L-shaped geometry and houses a single interferometer.

Exploring the sensitivity of next generation gravitational wave detectors
B P Abbott et al 2017 CQG. 34 044001

Frequency-dependent responses in third generation gravitational-wave detectors
Essick, Vitale, Evans PRD **96**, 084004 (2017)
Theoretical physics implications of gravitational wave observation with future detectors
Chamberlain and Yunes PRD **96**, 084039 (2017)

LISA: the Space Detector

(Accepted :January 2017)

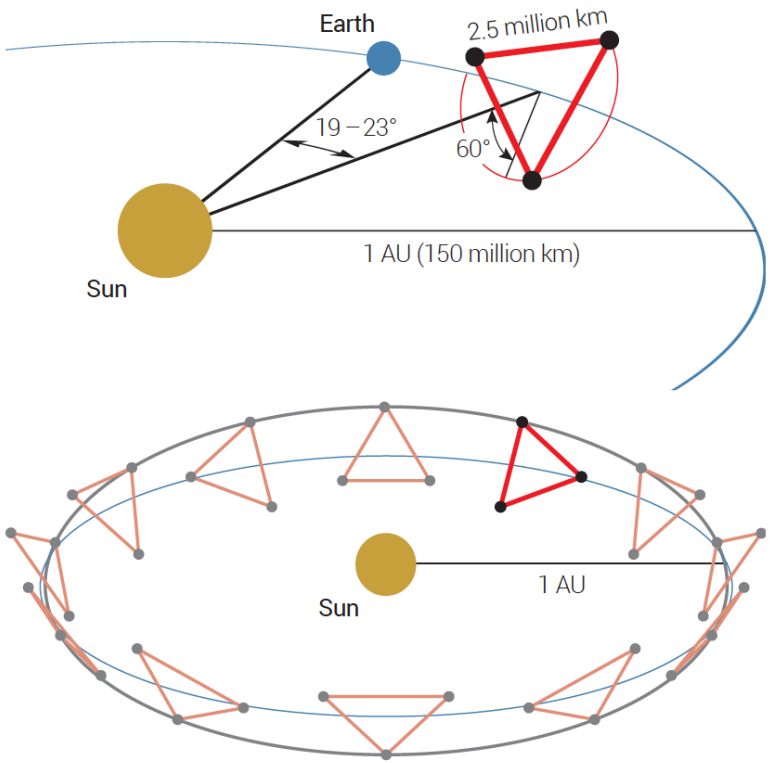

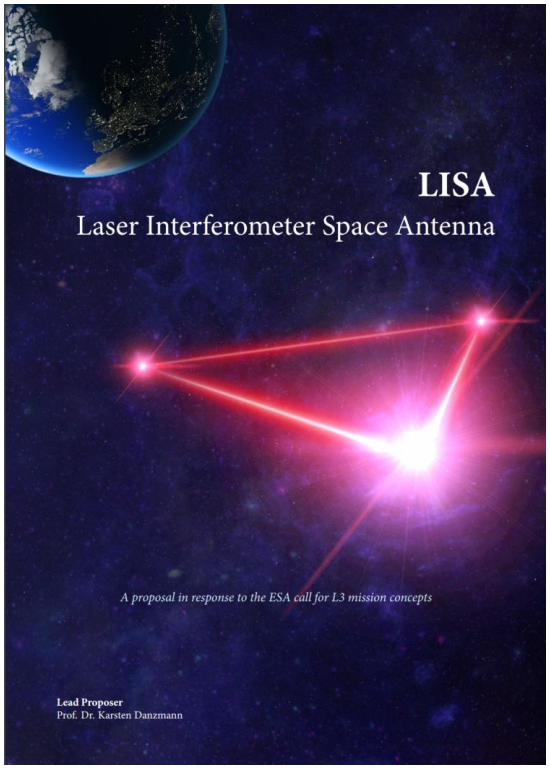

The Gravitational Wave Spectrum

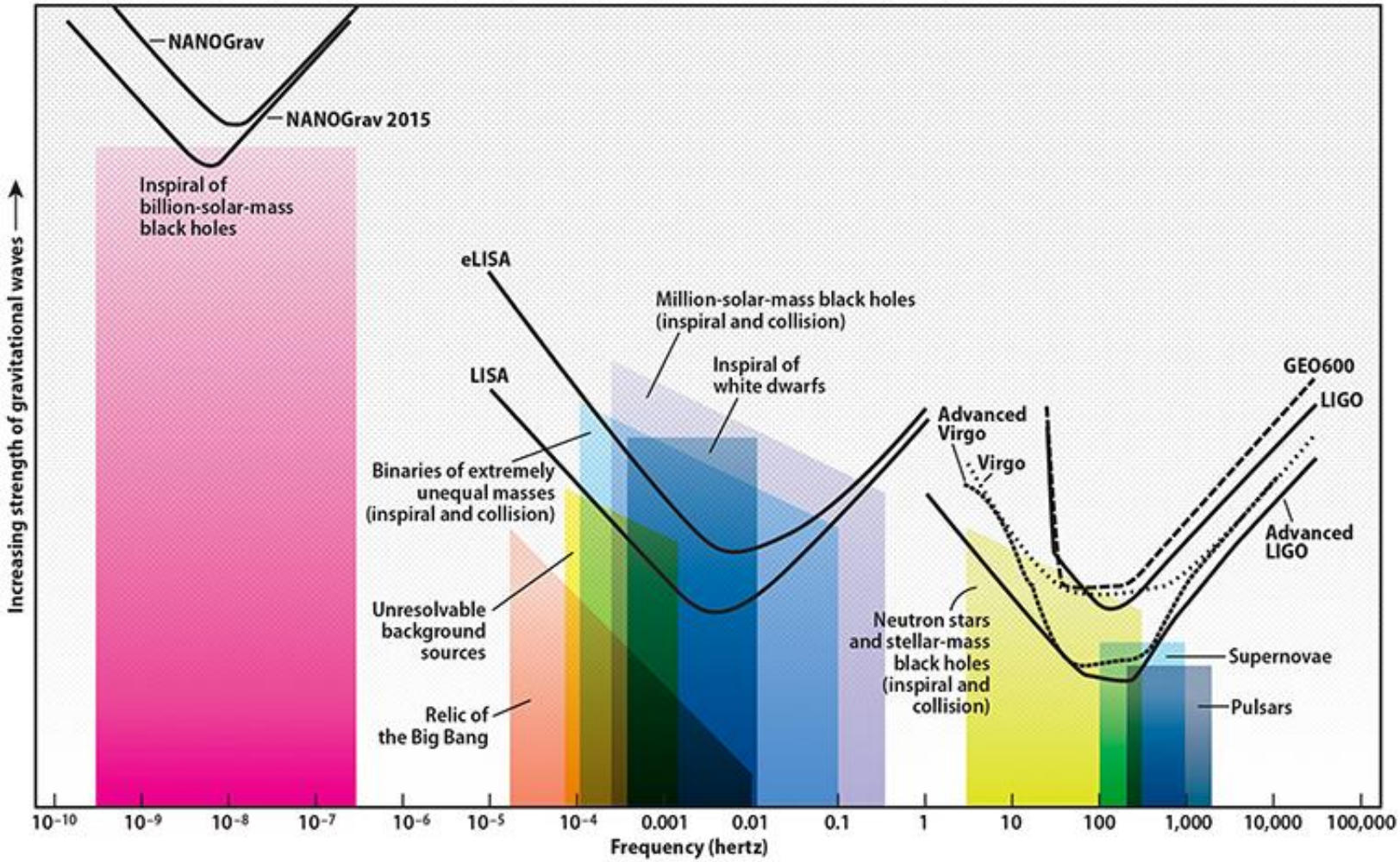

BH Ringdown (quasi-normal modes)

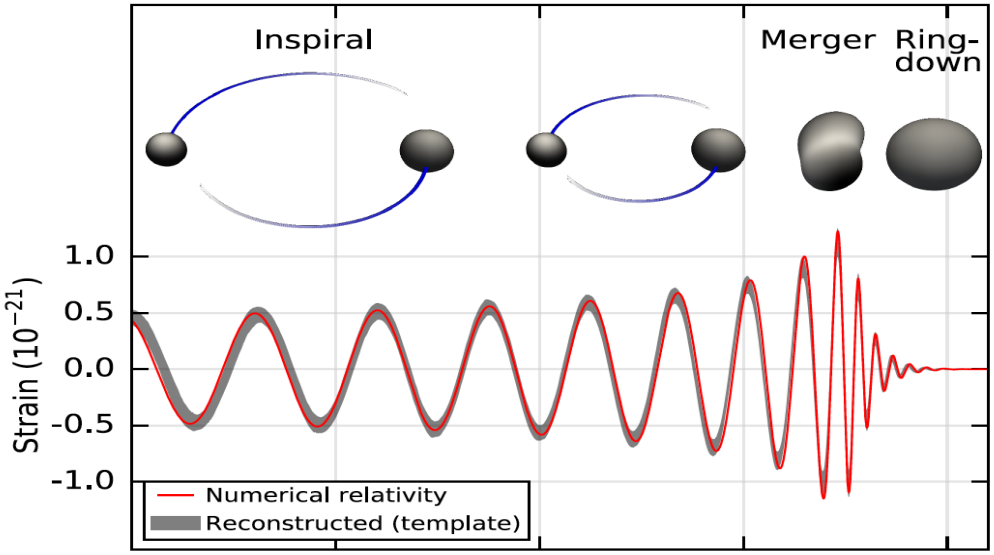

Inspiral-merger-ringdown search helps to disentangle the correlation between different parameters.

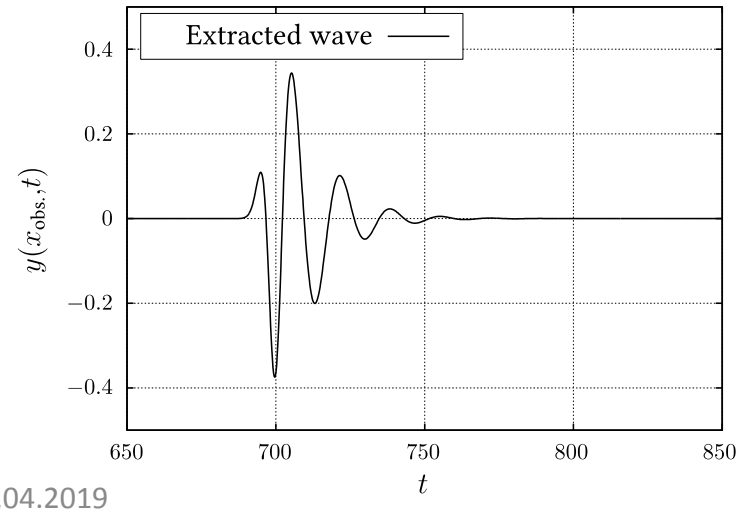

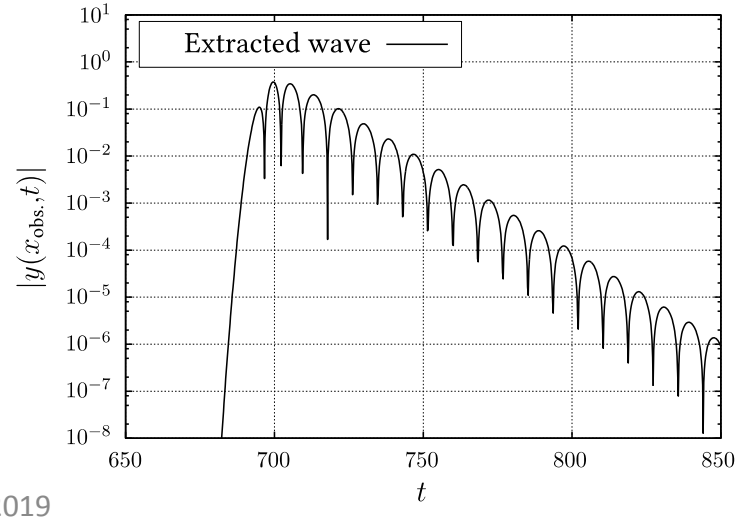

BH Ringdown (quasi-normal modes)

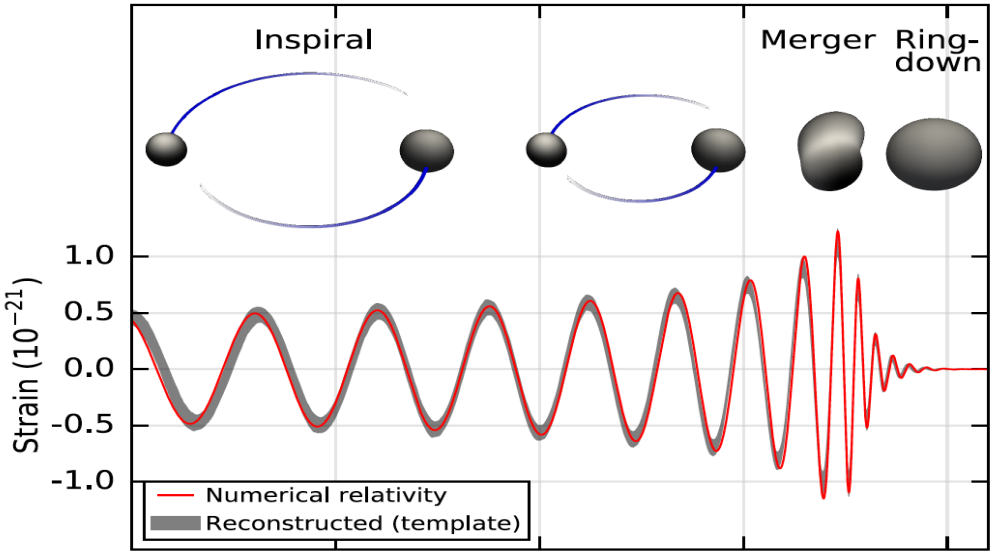

Inspiral-merger-ringdown search helps to disentangle the correlation between different parameters.

- **Theoretically** even a single QNM can provide exact estimation of the BH parameters (M,a).
- **In practise**, the fast damping reduces the accuracy and extra modes need to be identified.

$$M\omega \approx \left[1 - \frac{63}{100}(1-a)^{3/10}\right] \approx (0.37 + 0.19a),$$

$$\tau \approx \frac{4M}{(1-a)^{9/10}}\left[1 - \frac{63}{100}(1-a)^{3/10}\right]^{-1} \approx M(1.48 + 2.09a).$$

BH Ringdown vs Inspiral

LIGO: "Tests of GR with Binary BH signals" (1903.04467)

Inspiral-merger-ringdown search helps to disentangle the correlation between different parameters.

Event	Properties				FAR			SNR	GR tests performed				
	D_L [Mpc]	M_{tot} [$M_\odot$]	M_f [$M_\odot$]	a_f	PyCBC [yr^{-1}]	GstLAL [yr^{-1}]	cWB [yr^{-1}]		RT	IMR	PI	PPI	MDR
GW150914[b]	430^{+150}_{-170}	$66.2^{+3.7}_{-3.3}$	$63.1^{+3.3}_{-3.0}$	$0.69^{+0.05}_{-0.04}$	$< 1.5 \times 10^{-5}$	$< 1.0 \times 10^{-7}$	$< 1.6 \times 10^{-4}$	$25.3^{+0.1}_{-0.2}$	✓	✓	✓	✓	✓
GW151012[b]	1060^{+550}_{-480}	$37.3^{+10.6}_{-3.9}$	$35.7^{+10.7}_{-3.8}$	$0.67^{+0.13}_{-0.11}$	0.17	7.9×10^{-3}	–	$9.2^{+0.3}_{-0.4}$	✓	–	–	✓	✓
GW151226[b,c]	440^{+180}_{-190}	$21.5^{+6.2}_{-1.5}$	$20.5^{+6.4}_{-1.5}$	$0.74^{+0.07}_{-0.05}$	$< 1.7 \times 10^{-5}$	$< 1.0 \times 10^{-7}$	0.02	$12.4^{+0.2}_{-0.3}$	✓	–	✓	–	✓
GW170104	960^{+440}_{-420}	$51.3^{+5.3}_{-4.2}$	$49.1^{+5.2}_{-4.0}$	$0.66^{+0.08}_{-0.11}$	$< 1.4 \times 10^{-5}$	$< 1.0 \times 10^{-7}$	2.9×10^{-4}	$14.0^{+0.2}_{-0.3}$	✓	✓	✓	✓	✓
GW170608	320^{+120}_{-110}	$18.6^{+3.1}_{-0.7}$	$17.8^{+3.2}_{-0.7}$	$0.69^{+0.04}_{-0.04}$	$< 3.1 \times 10^{-4}$	$< 1.0 \times 10^{-7}$	1.4×10^{-4}	$15.6^{+0.2}_{-0.3}$	✓	–	✓	✓	✓
GW170729[d]	2760^{+1380}_{-1340}	$85.2^{+15.6}_{-11.1}$	$80.3^{+14.6}_{-10.2}$	$0.81^{+0.07}_{-0.13}$	1.4	0.18	0.02	$10.8^{+0.4}_{-0.5}$	✓	✓	–	✓	✓
GW170809	990^{+320}_{-380}	$59.2^{+5.4}_{-3.9}$	$56.4^{+5.2}_{-3.7}$	$0.70^{+0.08}_{-0.09}$	1.4×10^{-4}	$< 1.0 \times 10^{-7}$	–	$12.7^{+0.2}_{-0.3}$	✓	✓	–	✓	✓
GW170814	580^{+160}	$56.1^{+3.4}$	$53.4^{+3.2}$	$0.72^{+0.07}$	$< 1.2 \times 10^{-5}$	$< 1.0 \times 10^{-7}$	$< 2.1 \times 10^{-4}$	$17.8^{+0.3}$	✓	✓	✓	✓	✓

"…do not reveal any inconsistency of our data with the predictions of GR."

- **The first two of these tests** check the self-consistency of the analysis.
  - **1st (PM)** checks that the residual remaining after subtracting the best-fit waveform is consistent with detector noise.
  - **2nd (IMR)** checks that the **final mass and spin inferred** from the low- and high-frequency parts of the signal are consistent.
- **The 3rd and 4th tests** introduce parameterized deviations in the waveform model and check that these deviations are consistent with their GR value of zero.
  - **In one test (PI)**, they are phenomenological modifications of the coefficients in a waveform model, including the post-Newtonian coefficients.
  - **In the other test (PPI),** the deviations are those arising from the propagation of GWs with a modified dispersion relation, including the dispersion due to a **massive graviton as a special case.**
- **5th test (MDR),** they also check whether the observed polarizations are consistent with being **purely tensor modes** (as expected in GR) as opposed to **purely scalar modes or vector modes**.

BH Ringdown vs Inspiral

LIGO: ”Tests of GR with Binary BH signals” (1903.04467)

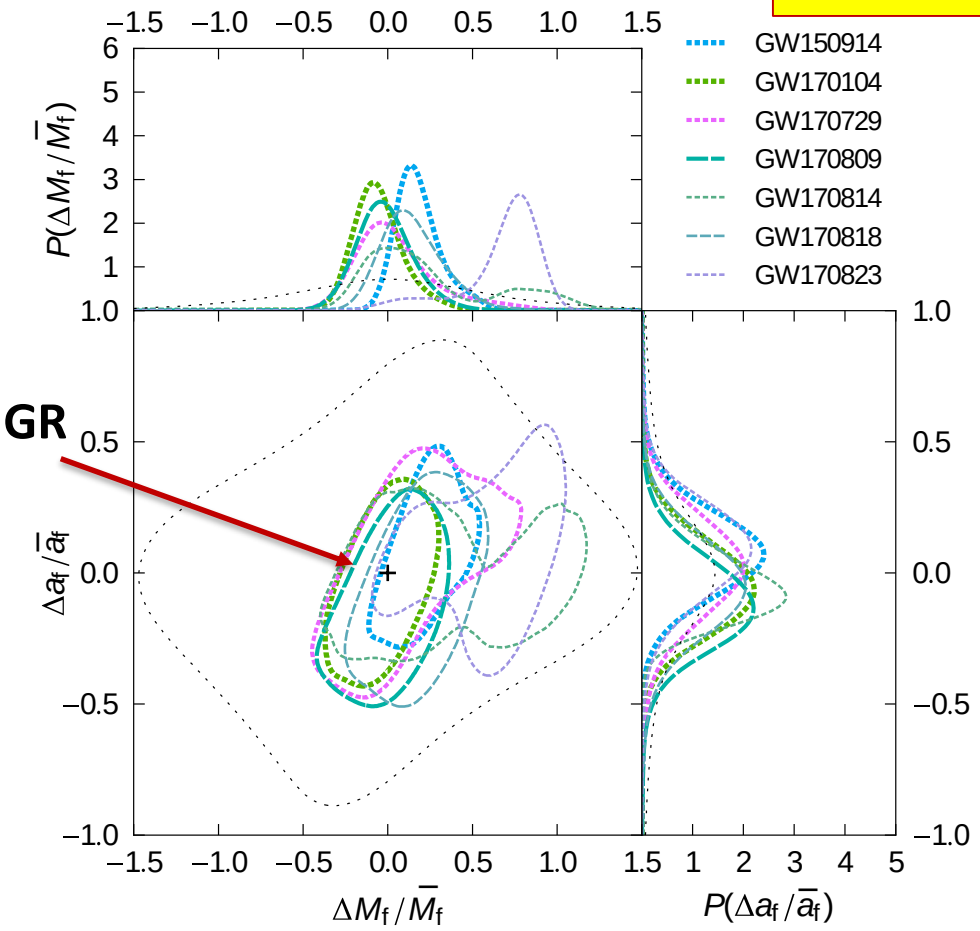

Results of the inspiral-merger-ringdown consistency test for the selected BBH events.

$$\frac{\Delta M_f}{\bar{M}_f} = \frac{2(M_f^{insp} - M_f^{post-insp})}{(M_f^{insp} + M_f^{post-insp})}$$

$$\frac{\Delta a_f}{\bar{a}_f} = \frac{2(a_f^{insp} - a_f^{post-insp})}{(a_f^{insp} + a_f^{post-insp})}$$

There is no statistically significant evidence for deviations from GR

“Echoes” from the “Abyss”

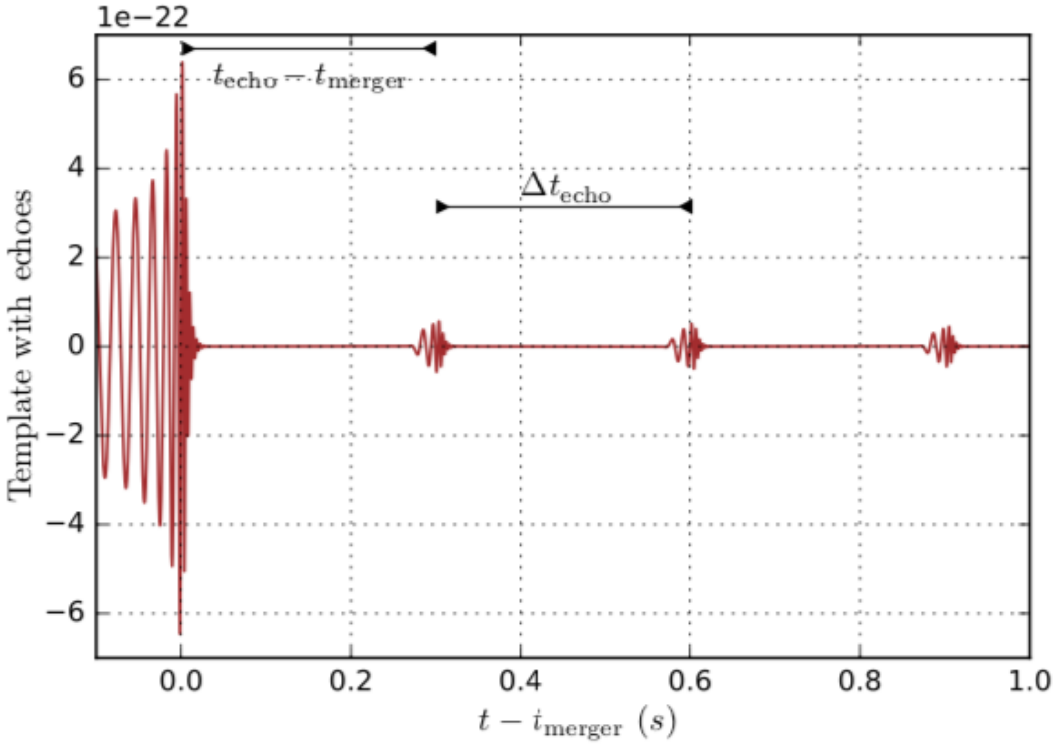

Abedi, Dykaar, Afshordi PRD (2017)

Searched for **observational signatures of echoes** in the GW data released by advanced LIGO following the 3 black hole merger events GW150914, GW151226, and LVT151012.

“Echoes” from the “Abyss”

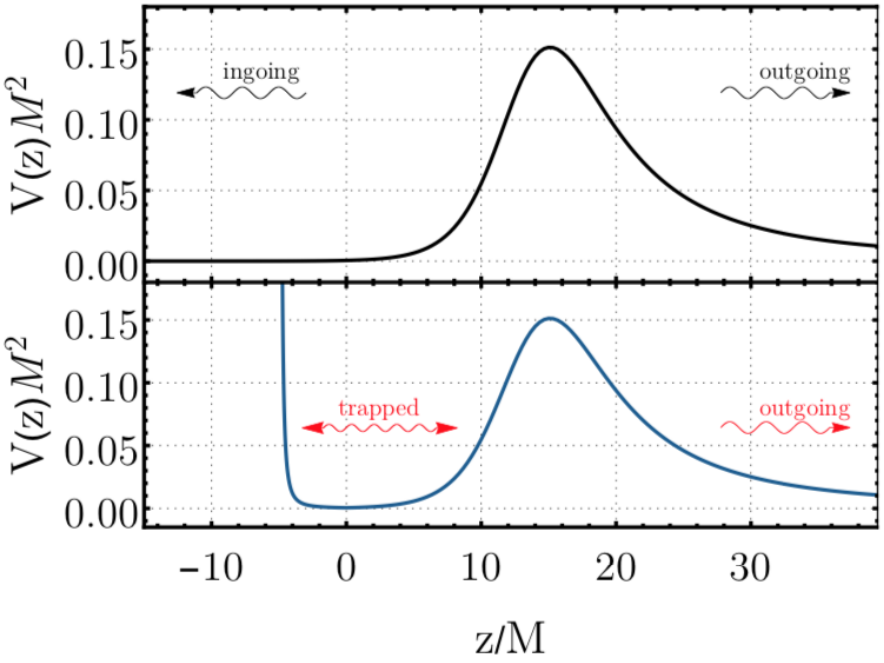

Typical effective potential

- For perturbations of **a Schwarzschild BH** (top panel)
- **A horizonless compact object**

The effective potential is peaked at **r ≈ 3M.**

- The BH QNMs are waves which are outgoing at infinity ($z \to +\infty$) and ingoing at the horizon ($z \to -\infty$),
- The presence of a potential well (provided either by a partly reflective surface, a centrifugal barrier at the center, or by the geometry) supports quasi-trapped, long-lived modes.

“Echoes” from the “Abyss”

A toy model of the mid 90s ... **KK 1995**

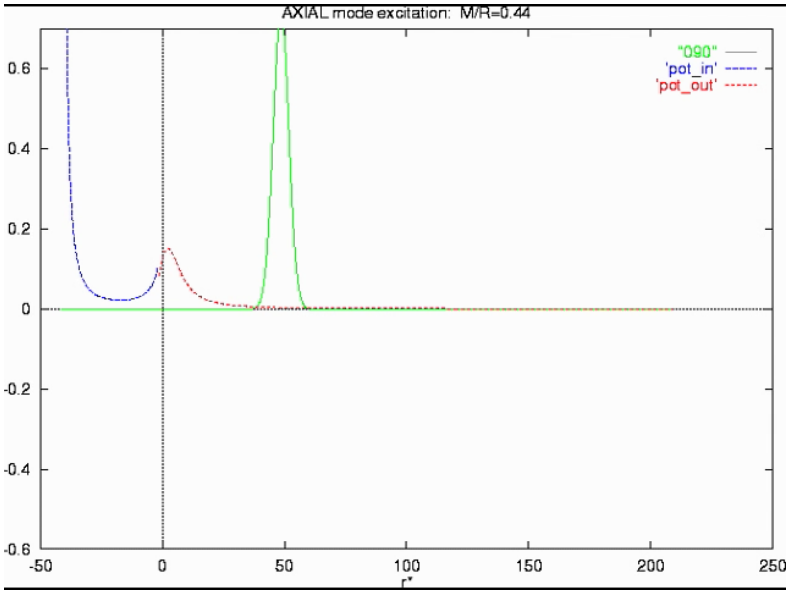

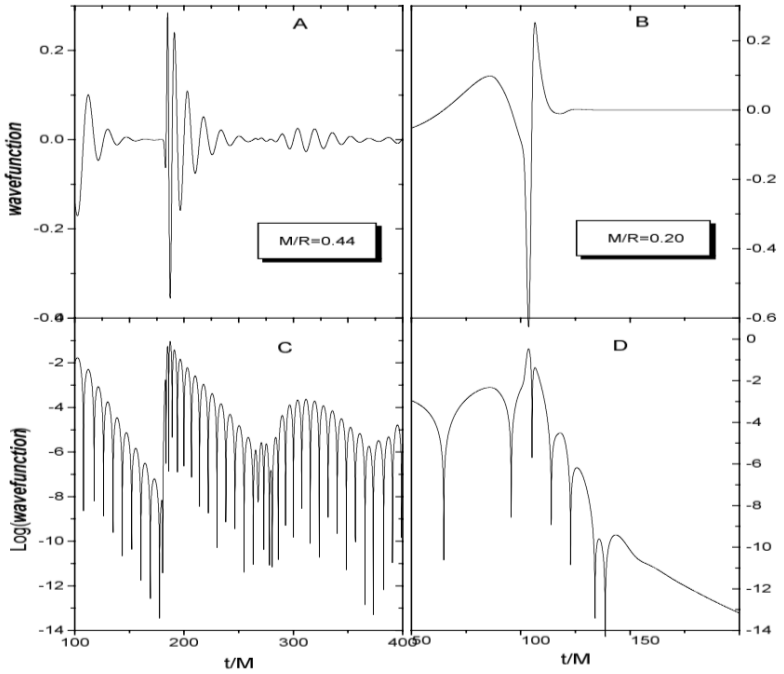

- **Boson Stars**
- **Anisotropic Stars**
- **Wormholes**
- **Gravastars**

...

“Echoes” from the “Abyss”

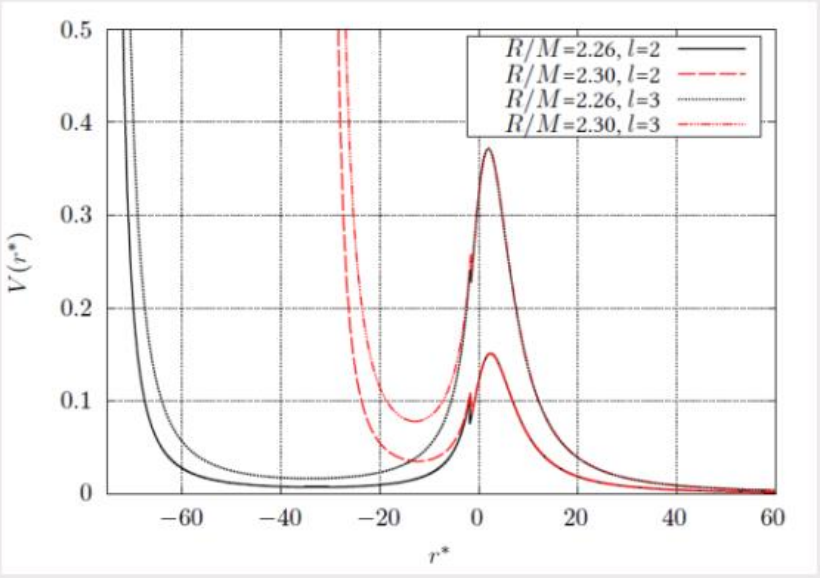

— FIG. 1. The axial mode potential for constant density stars with varying compactness R/M and angular decomposition parameter l. Figure taken from [18] S. H. Völkel and K. D. Kokkotas, Classical and Quantum Gravity 34, 125006 (2017),

Völkel-KK (2017-2019)

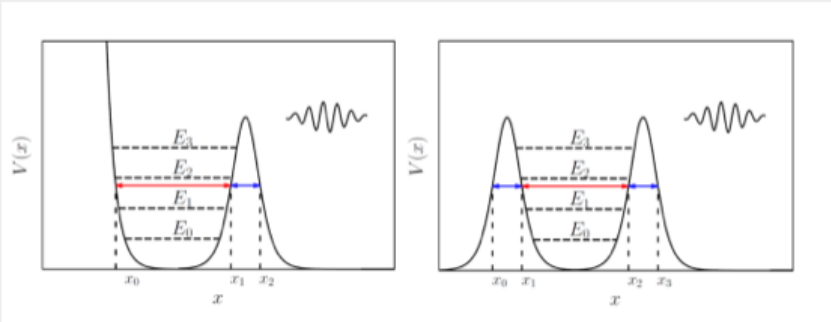

— FIG. 2. The two different types of potentials that appear in ultra compact stars on the left and in some wormholes on the right. The reconstructed potentials are derived as functions of their widths ($\mathscr{L}_1$, $\mathscr{L}_2$) (red, blue) assuming a known spectrum E_n.

GWs from Collapse

Richers etal PRD 2017

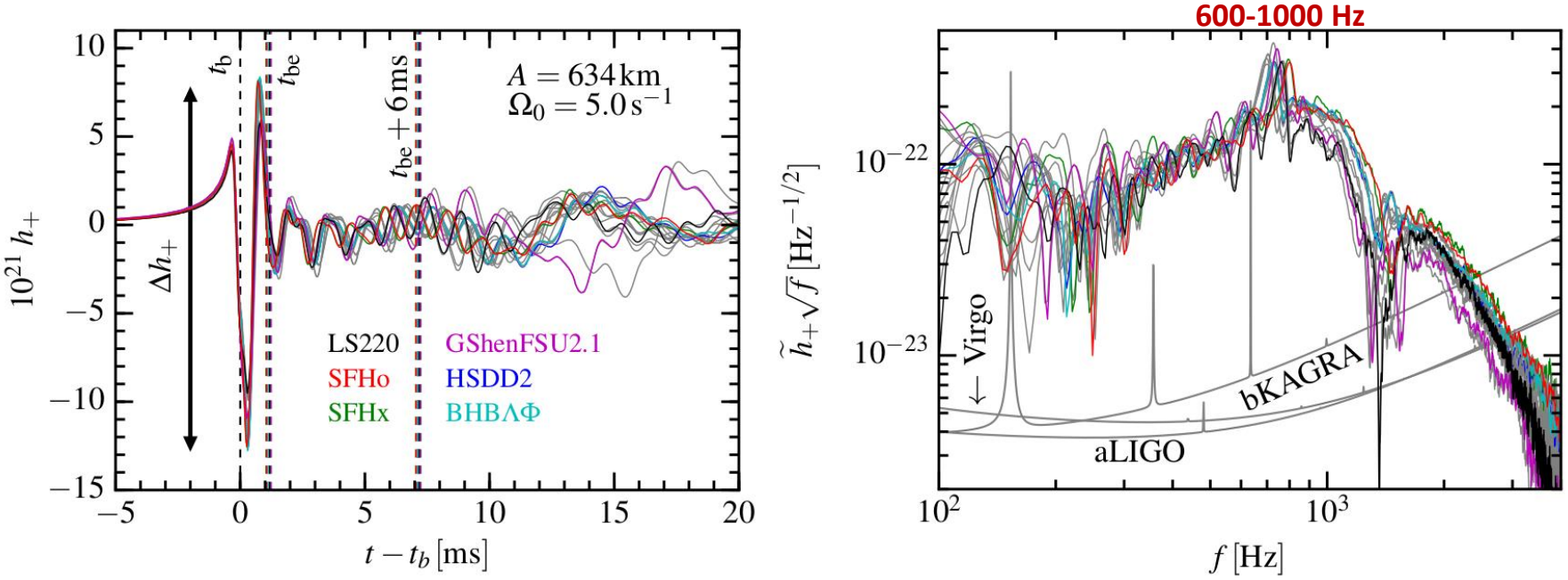

The time-domain waveforms (left panel) and Fourier transforms scaled by f (right panel) of signals from all 18 EOS for a moderately rotating core collapse. **Distance 10kpc**

t_b is the bounce time,

t_{be} is the end of the bounce signal, and

Δh_+ is the amplitude of the bounce signal.

The frequency of the post-bounce oscillations can be seen at the peak of each spectrum.

GWs from Collapse

Galactic neighbourhood signals, in the best case Virgo cluster

A few per century !!!

- Core Collapse, Bounce, and Rotation (instabilities)
- Convection (~500 Hz) $<10^{-10}\, M_{\odot}\, c^2$
- Fluid Oscillations (f-, p-, g-modes) (300-3000Hz) $\sim 10^{-10} - 10^{-8}\, M_{\odot}\, c^2$
- Standing Accretion Shock Instability (SASI)
- Mass Accretion
- ...

Excellent source for multi-messenger observations (Gravitational Waves, Neutrinos, and Electromagnetic waves)

The Many Faces of Neutron Stars

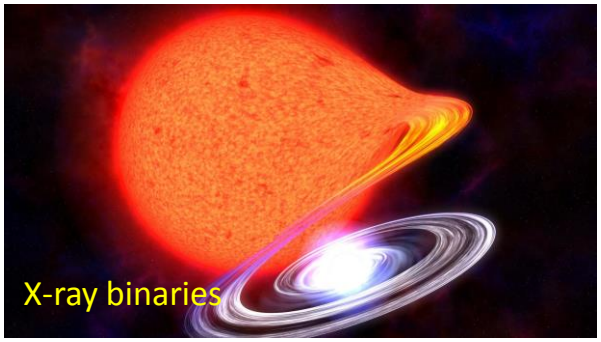

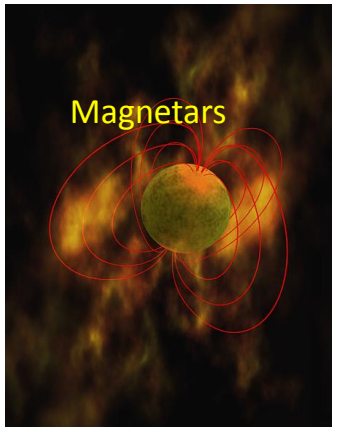

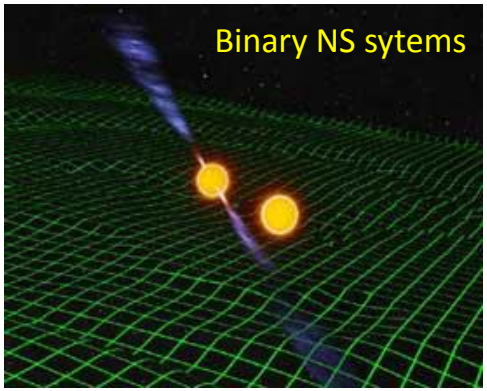

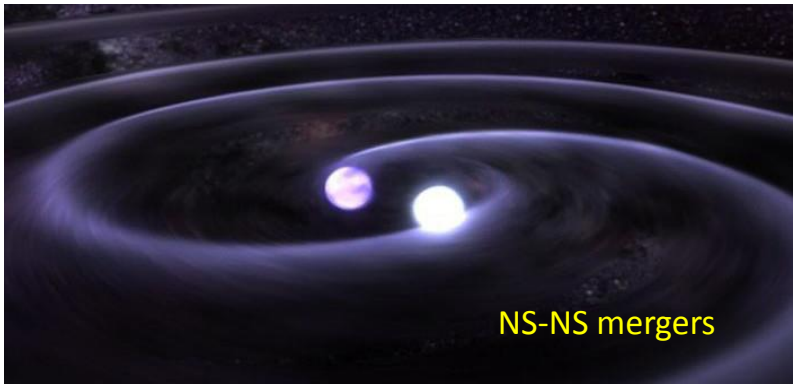

Typical masses ~1.2-2 $M_{\odot}$
Typical Radius ~9-14 km

Neutron Stars: Mass vs Radius

Static Models

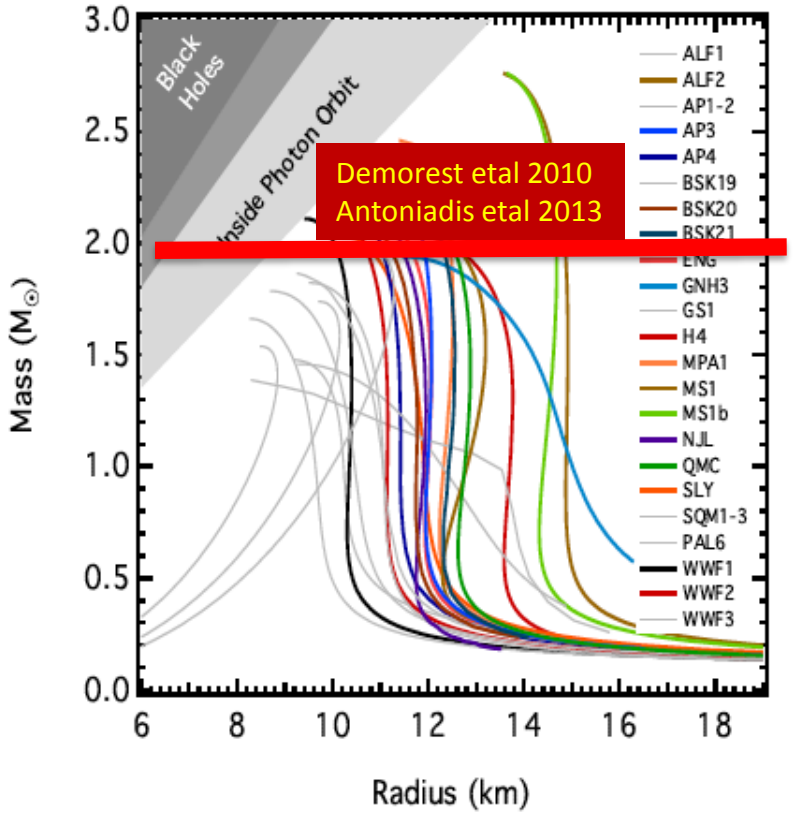

Özel & Freire (2016)

Rotating Models

supramassive

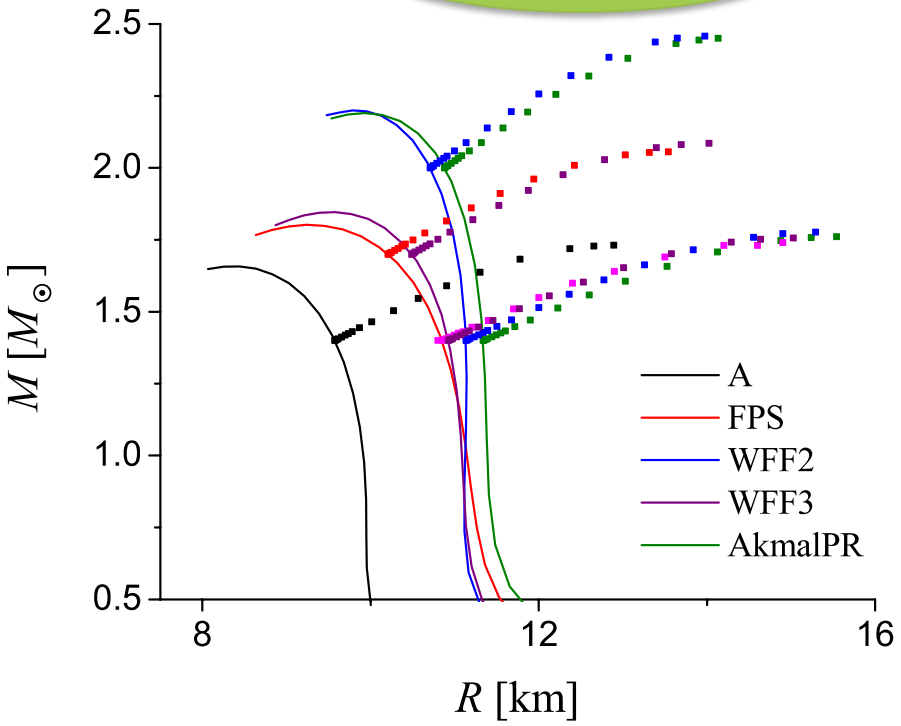

$$M_{max} \simeq 1.2\, M_{TOV}$$

Constraints on Neutron Star Radius
GW observations

Main methods in EM spectrum

- Thermonuclear X-ray bursts (photospheric radius expansion)
- Burst oscillations (rotationally modulated waveform)
- Fits of thermal spectra to cooling neutron stars
- khZ QPOs in accretion disks around neutron stars
- Pericenter precession in relativistic binaries (double pulsar J0737)

Main methods in GW spectrum

- Tidal effects on waveform during inspiral phase of NS-NS mergers
- Tidal disruption in BH-NS mergers
- Oscillations in (early & late) post-merger phase
- Oscillation in the post-collapse phase

Equation of State:
Constraints from X-ray binaries / bursts

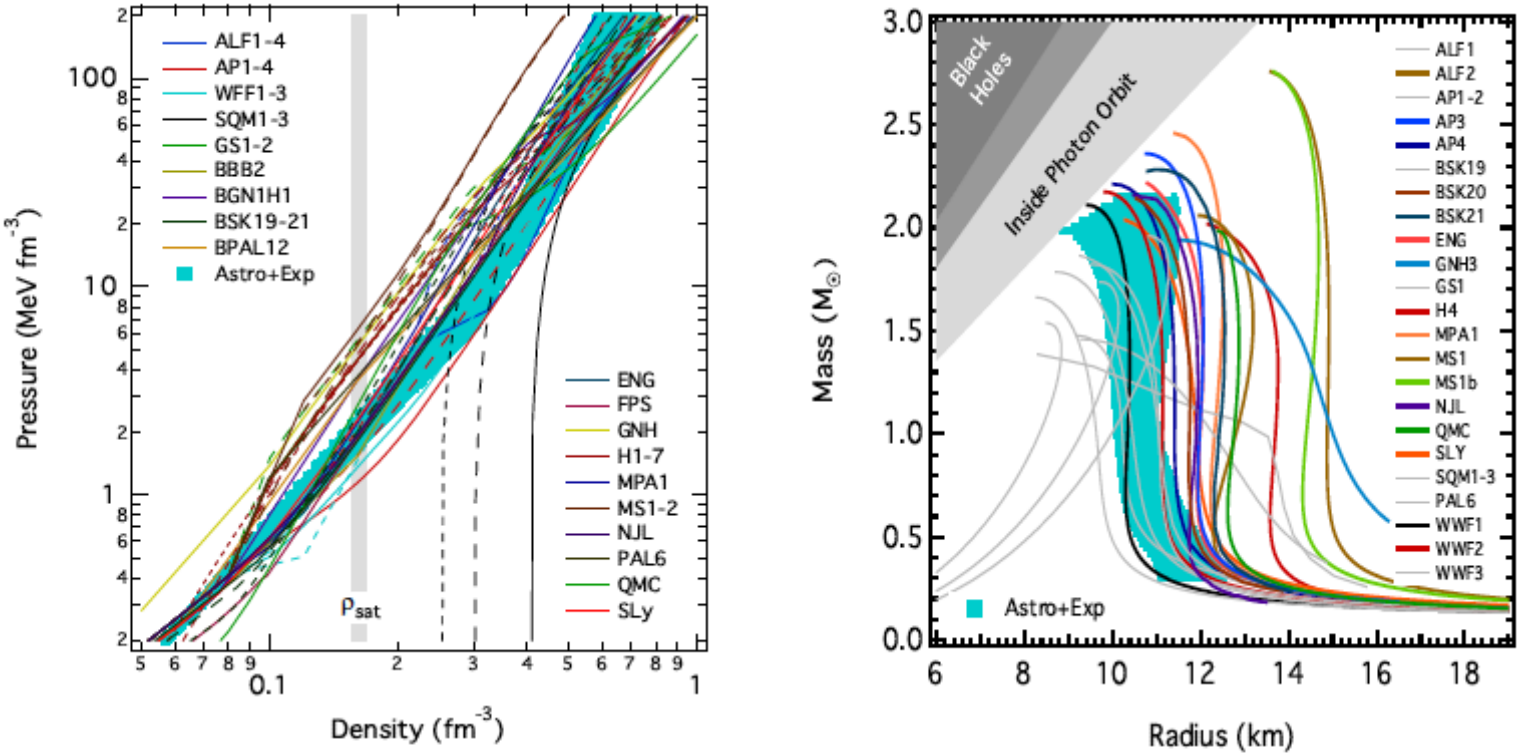

Figure 10

The astrophysically inferred (left) EoS and (right) mass-radius relation corresponding to the most likely triplets of pressures that agree with all of the neutron star radius and low energy nucleon-nucleon scattering data and allow for a $M > 1.97\ M_\odot$ neutron star mass. The light blue bands show the range of pressures and the mass-radius relations that correspond to the region of the (P_1, P_2, P_3) parameter space in which the likelihood is within e^{-1} of its highest value. Around $1.5\ M_\odot$, this inferred EoS predicts radii between $9.9 - 11.2$ km.

Özel & Freire (2016)

Neutron Stars & "universal relations"

Need for relations between the "observables" and the "fundamentals" of NS physics

Average Density	$\bar{r} \sim M / R^3$	
Compactness	$z \sim M/R$	$h = \sqrt{M^3 / I}$
Moment of Inertia	$I \sim MR^2$	$I \sim J / \Omega$
Quadrupole Moment	$Q \sim R^5 \Omega^2$	
Tidal Love Numbers	$\lambda \sim I^2 Q$	

I-Love-Q relations

EOS independent relations were derived by **Yagi & Yunes(2013)** for non-magnetized stars in the slow-rotation and small tidal deformation approximations.

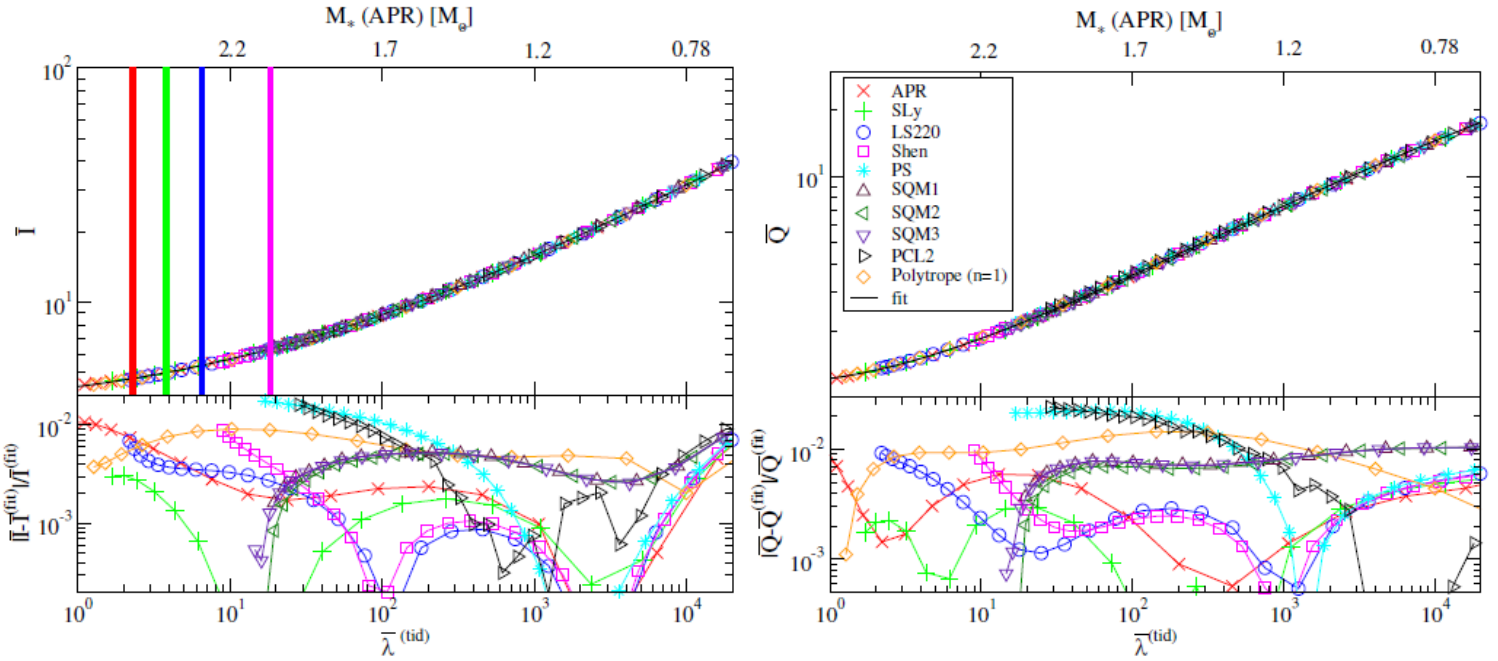

… the relations proved to be valid (*with appropriate normalizations*) even for *fast rotating* and *magnetized* stars

Latest developments: Yagi-Yunes arXiv:1601.02171 & arXiv:1608.06187

Oscillations & Instabilities

Gravitational Wave Asteroseismology

The most promising strategy for constraining the physics of neutron stars involves observing their "ringing" (oscillation modes)

- **f-mode :** scales with average density
- **p-modes:** probes the sound speed through out the star
- **g-modes :** sensitive to thermal/composition gradients
- **i-modes:** inertial modes associated with rotation (r-mode)
- **w-modes:** oscillations of spacetime itself.
- **s-modes:** Shear waves in the crust
- **Alfvèn modes:** due to magnetic field

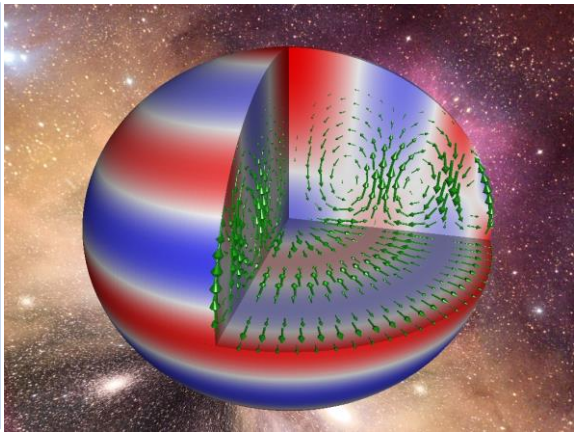

Typically **SMALL AMPLITUDE** oscillations –> weak emission of GWs

UNLESS

they become **unstable due to rotation** (r-mode & f-mode)

$l = 2, m = 2$

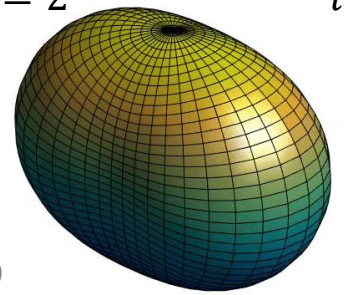

$l = 3, m = 3$

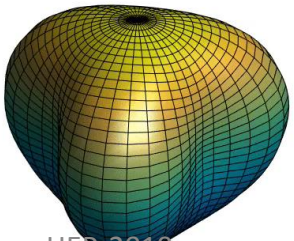

$l = 4, m = 4$

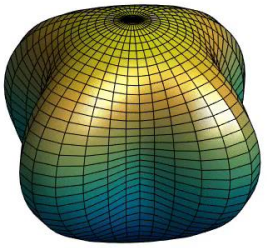

GW Asteroseismology: f-modes

$$M\omega_i^{unst} = \left[(0.56 - 0.94\ell) + (0.08 - 0.19\ell)M\Omega + 1.2(\ell+1)h\right]$$

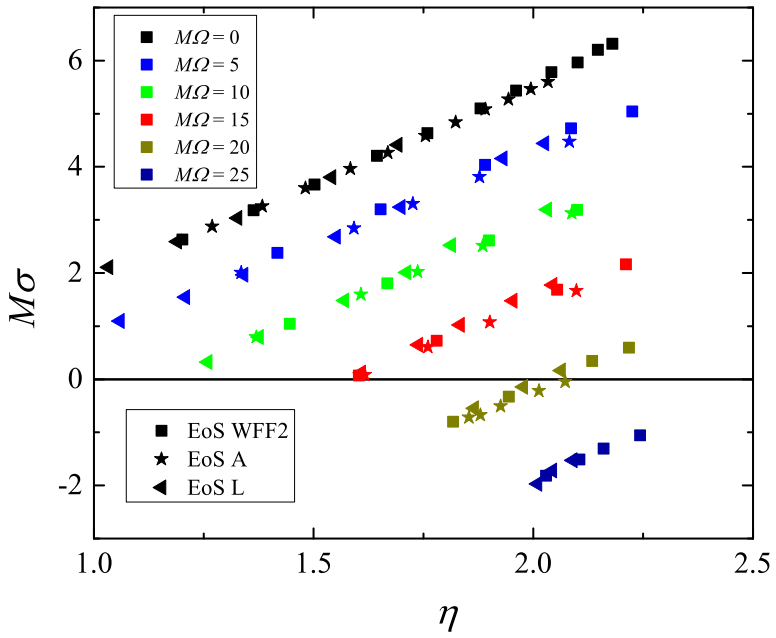

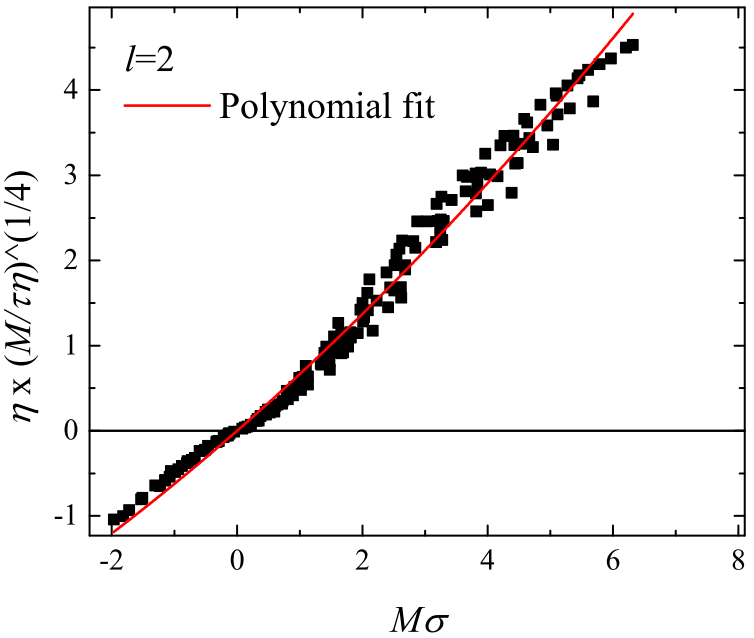

The $\ell = 2$ f-mode oscillation frequencies and damping as functions of the parameter η (moment of inertia)

$$h = \sqrt{M^3 / I}$$

Doneva-Kokkotas 2015

Binary Neutron Star Mergers
the standard scenario

The GW signal can be divided into **three distinct phases**

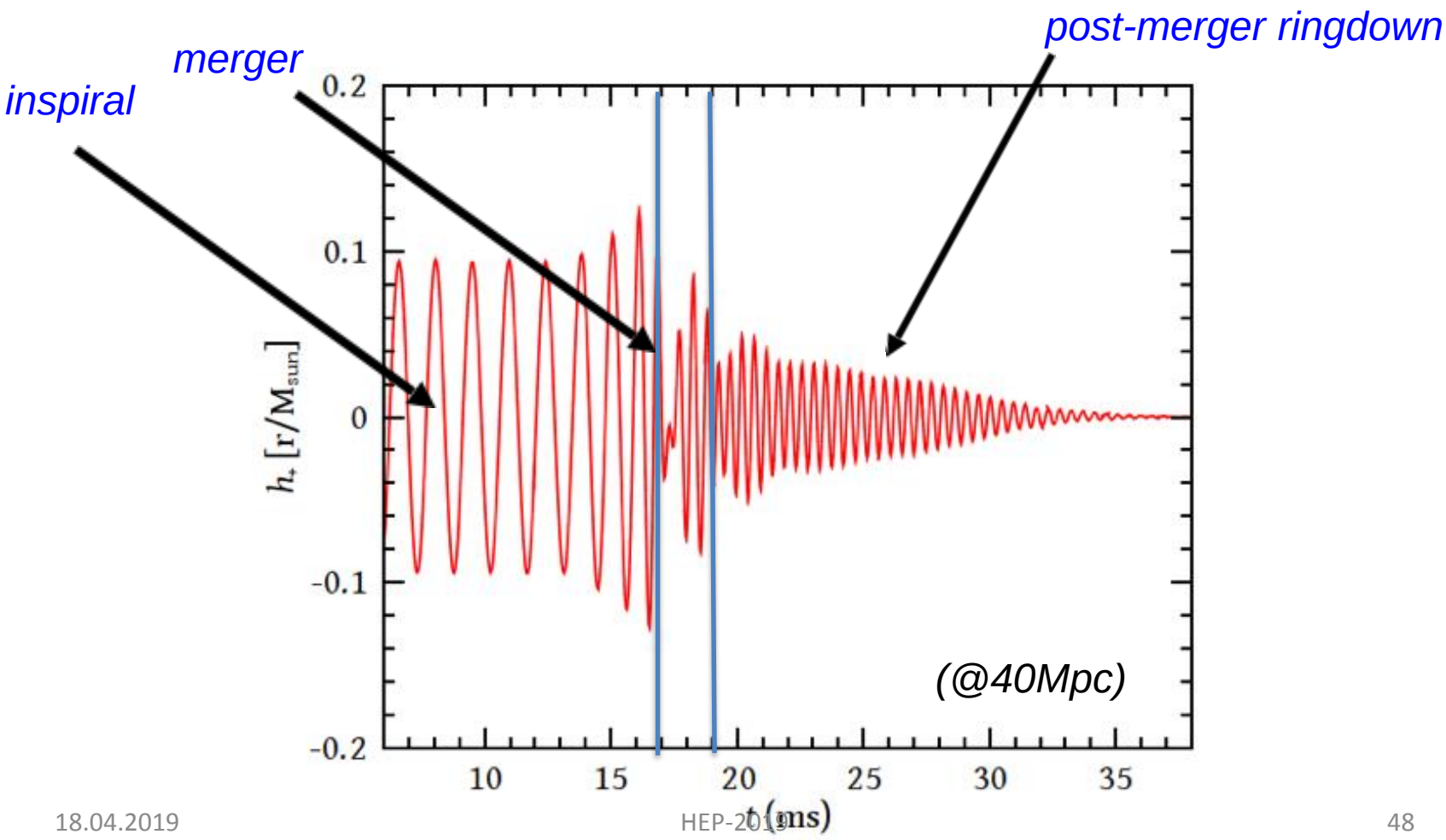

Binary Neutron Star Mergers
the post-Merger scenario

I. Direct collapse to BH if
$$M_{TOT} > M_{max}(\Omega)$$

II. Formation of an "unstable" NS if
$$M_{max}(\Omega) > M_{TOT} > M_{max}$$

III. Formation of a "stable" NS if
$$M_{TOT} < M_{max}(\Omega)$$

- NS-NS mergers will produce: Gao, Zhang, Lü 2016
  - ~40% prompt BHS
  - ~30% supramassive NS -> BH
  - ~30% Stable NS
- Initial spin near breakup limit ~1ms

Differential rotation/turbulence -->
strongly twisted internal field $E_B \geq 10^{50} erg$

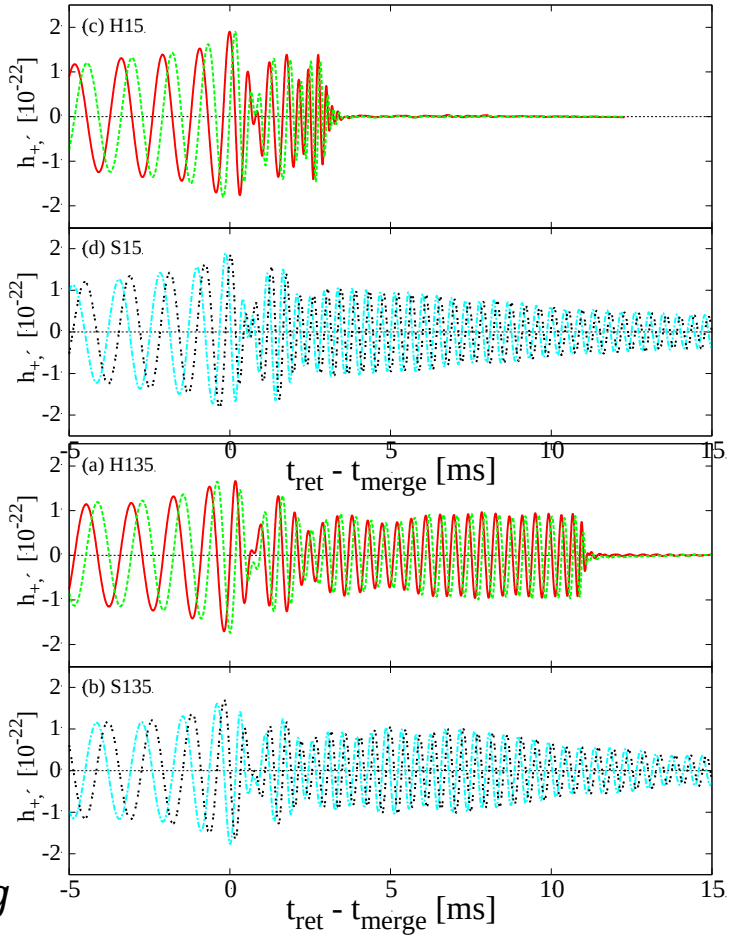

e.g. Rosswog etal (2003), Rezzolla etal 2011, Kiuchi etal 2012, Giacomazzo & Perna 2013, Giacomazzo etal 2015, Kyotoku etal 2015,…

Kiuchi, Sekiguchi, Kyutoku, Shibata 2012

Binary Neutron Star Mergers
Tidal Interaction

Tidal interactions affect the last part of the inspiral, modifying the orbital motion and the GW emission.

Kokkotas-Schaefer MNRAS 1995

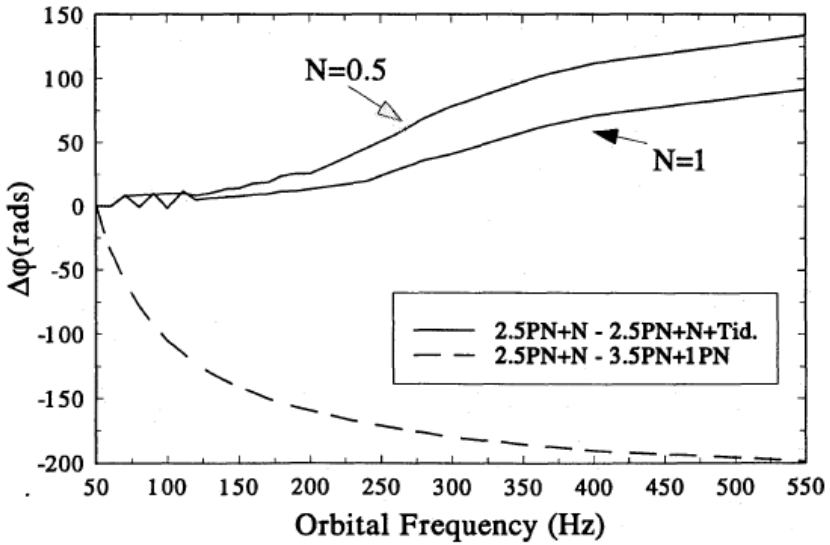

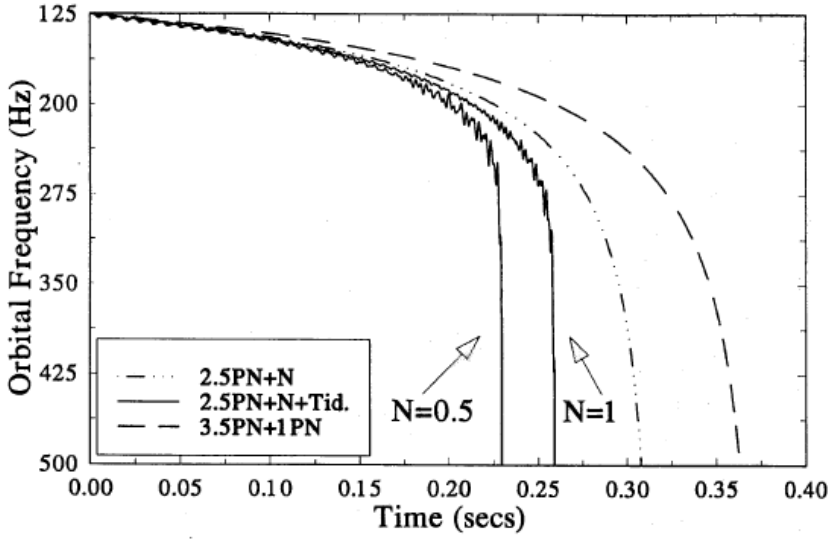

Bildsten-Cutler 1992
Lai et al 1993,1994
Kokkotas-Schaefer 1993-5
Shibata 1994
Flanagan 1998
Ho-Lai 1999
…

Binary Neutron Star Mergers
Tidal Interaction

Tidal interactions affect the last part of the inspiral, modifying the orbital motion and the GW emission.

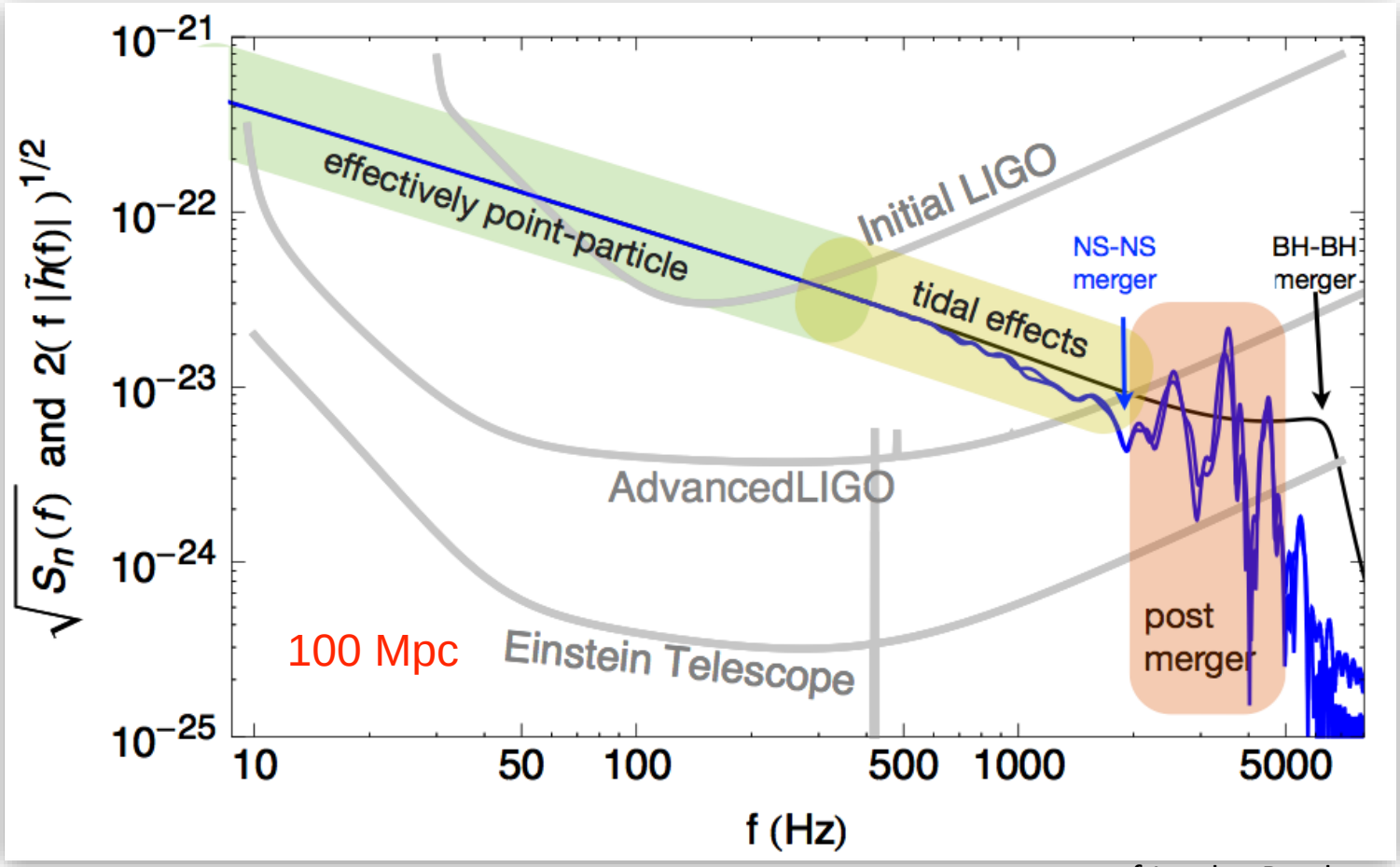

courtesy of Jocelyn Read

Binary Neutron Star Mergers
Tidal Love numbers

The last part of the inspiral signal carries the imprint of the quadrupole tidal deformability

$$\lambda = -\frac{Q_{ij}}{E_{ij}} = \frac{2}{3} k_2 R^5$$

Read et al. (2013), Hotozaka et al (2013)…

k_2 : tidal Love number

$$\Lambda \equiv \frac{2}{3} k_2 \left(\frac{R}{M}\right)^5$$

The leading tidal contribution to the phase evolution is a combination of the two tidal parameters. It is of 5PN order

$$\tilde{\Lambda} = \frac{16}{13} \frac{(m_1 + 12m_2) m_1^4 \Lambda_1 + (m_2 + 12m_1) m_2^4 \Lambda_2}{(m_1 + m_2)^5}$$

Measurements of M_{NS} and Λ would be helpful to constrain the NS EOS

With aLIGO

$\frac{\Delta R}{R} \sim 10\%$ at 100Mpc

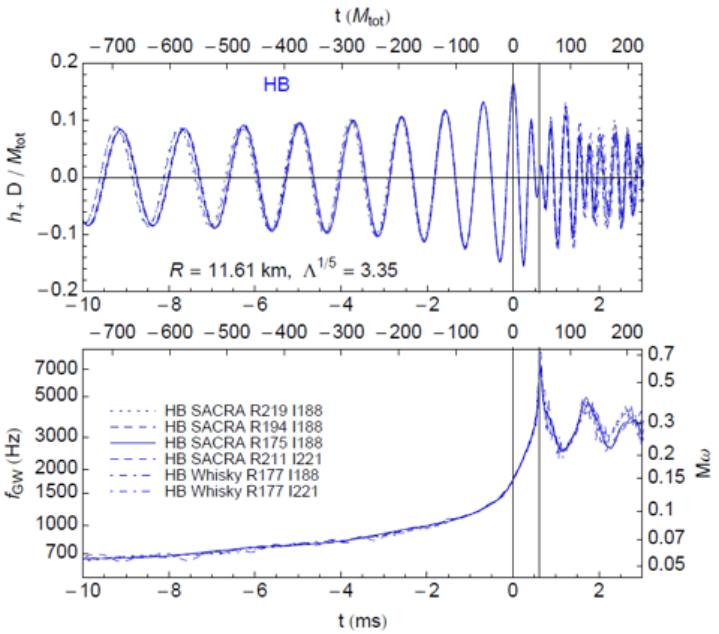

Binary Neutron Star Mergers
Tidal Interaction

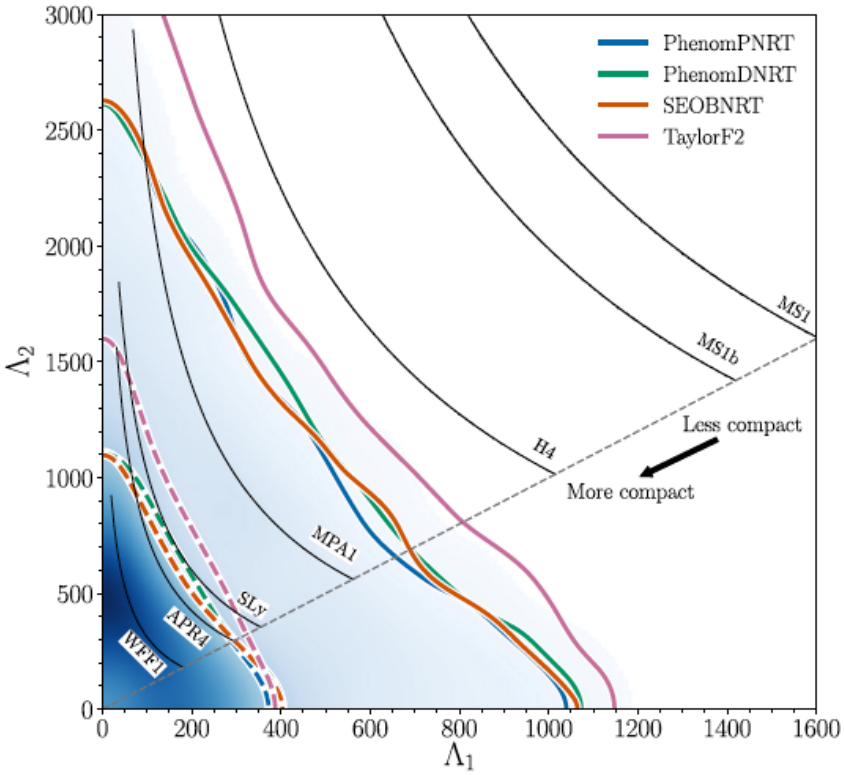

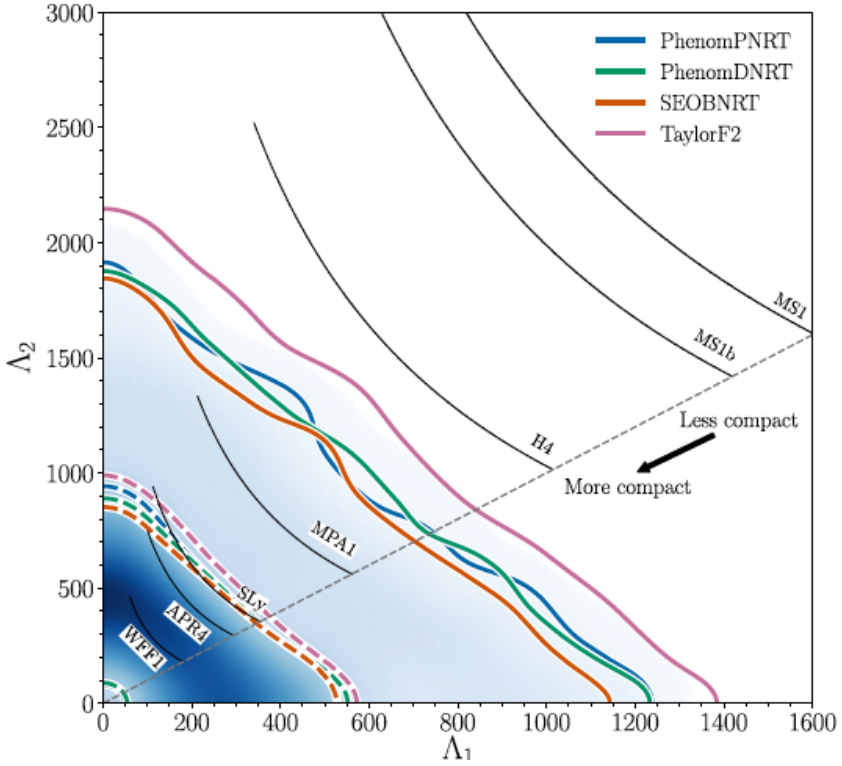

Probability density for the tidal deformability parameters of the *high spin* and *low spin* mass components inferred from the detected signals using the post-Newtonian model.

Equation of State:
Constraints from GW170817 (Bauswein etal)

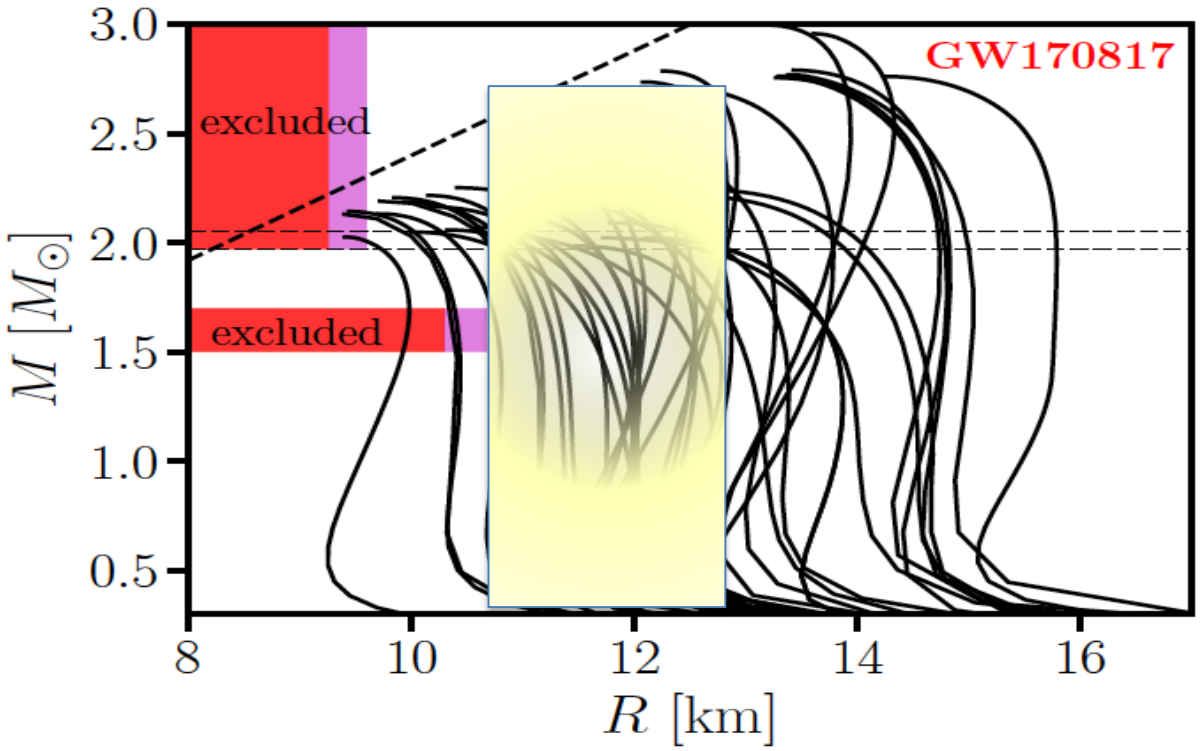

Figure 2. Mass-radius relations of different EoSs with very conservative (red area) and "realistic" (cyan area) constraints of this work for $R_{1.6}$ and $R_{\max}$. Horizontal lines display the limit by Antoniadis & et al. (2013). The dashed line shows the causality limit.

Equation of State:
Constraints from GW170817 (Rezzolla etal)

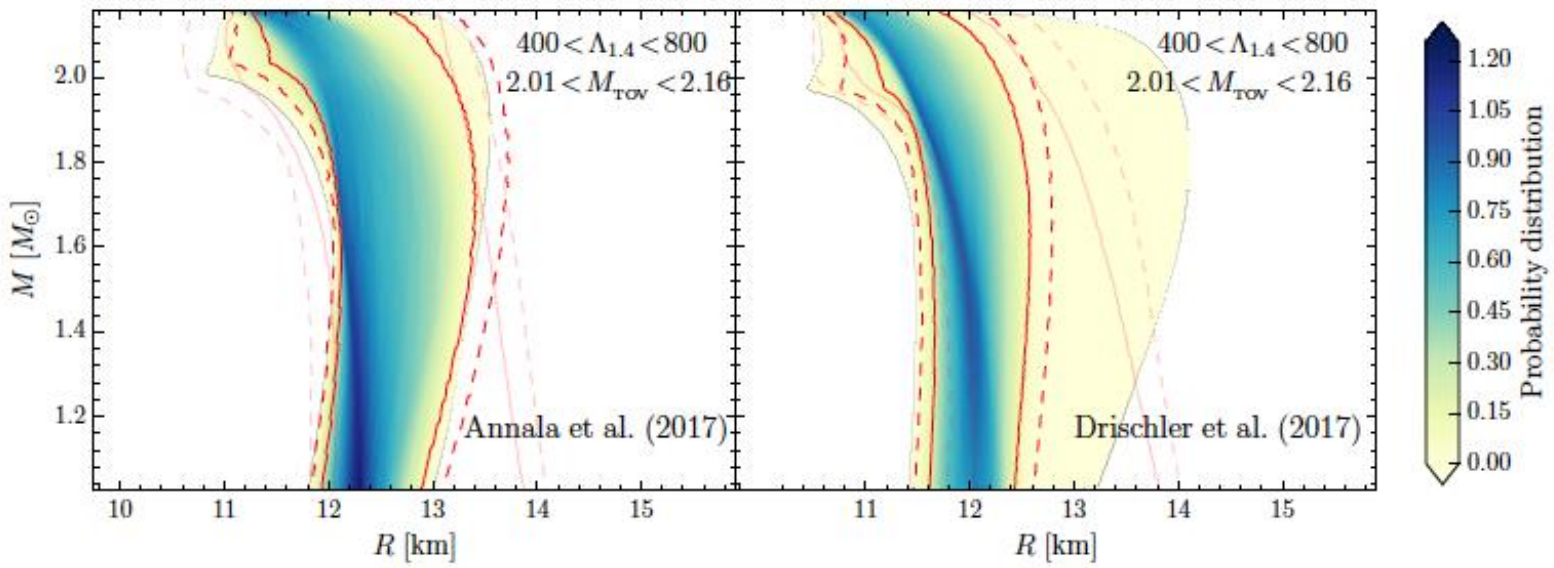

FIG. 4. *Left panel:* The same as in bottom-right panel of Fig. 1, but when the neutron matter in the outer core is treated following the approach of [11]. *Right panel:* The same as in the left panel but when considering the more recent prescription of [29] for the outer core. Shown as light shaded lines are the $2/3$-σ values reported in the bottom-right panel of Fig. 1.

Equation of State:
Constraints from GW170817 (Radice etal)

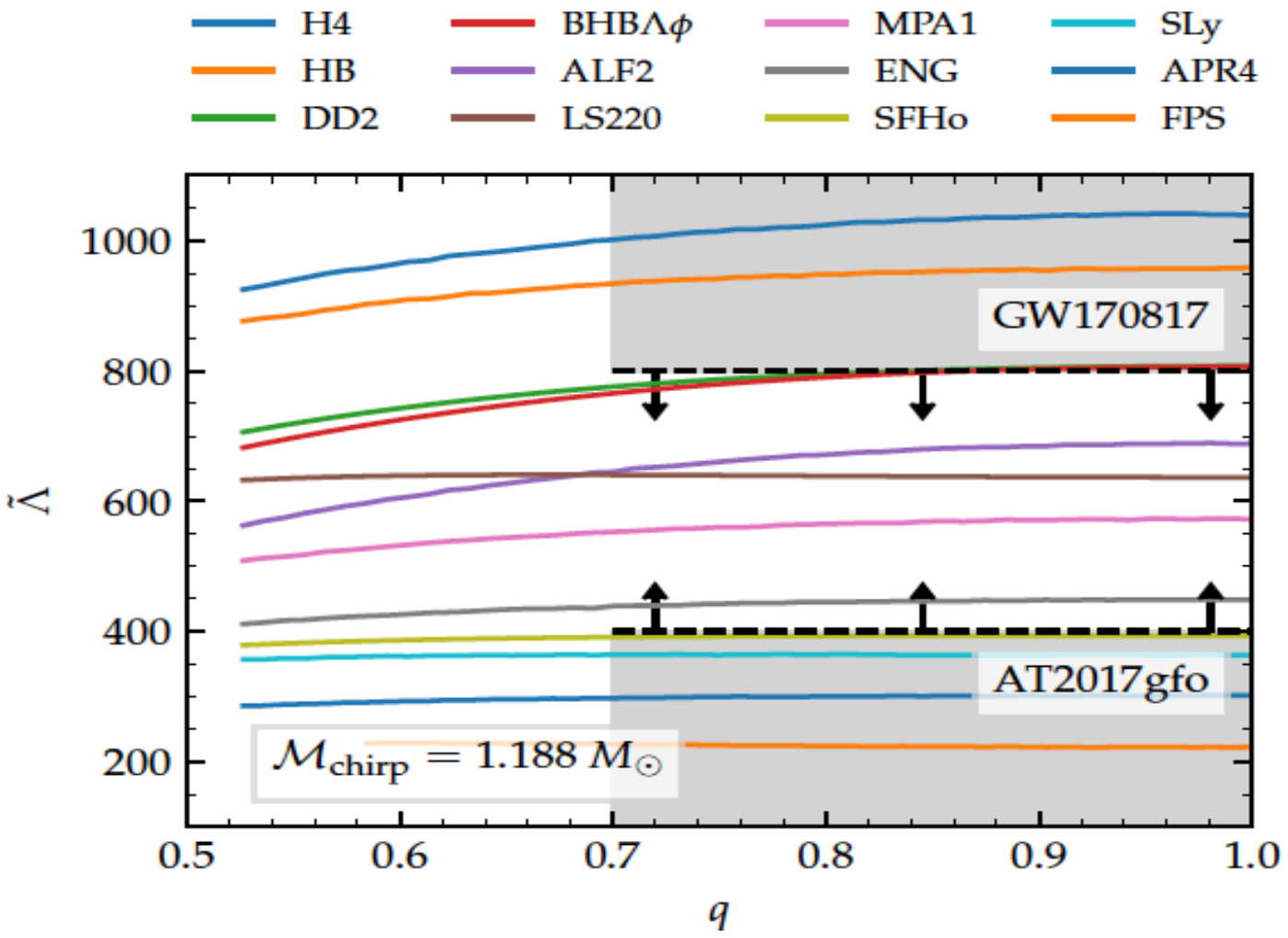

Binary NS merger rates

Constraints from GW170817

Using the BNS merger the LIGO–Virgo detection rate is narrowed down:

-- from **0.04–100** to **~1–50 BNS** coalescences during the O3

-- At design sensitivity, the LIGO/Virgo can expect to detect **~6–120 BNS** coalescences per year, as opposed to the previously estimated **0.1–200**

Any additional BNS detections in the meantime will allow this prediction to be further sharpened.

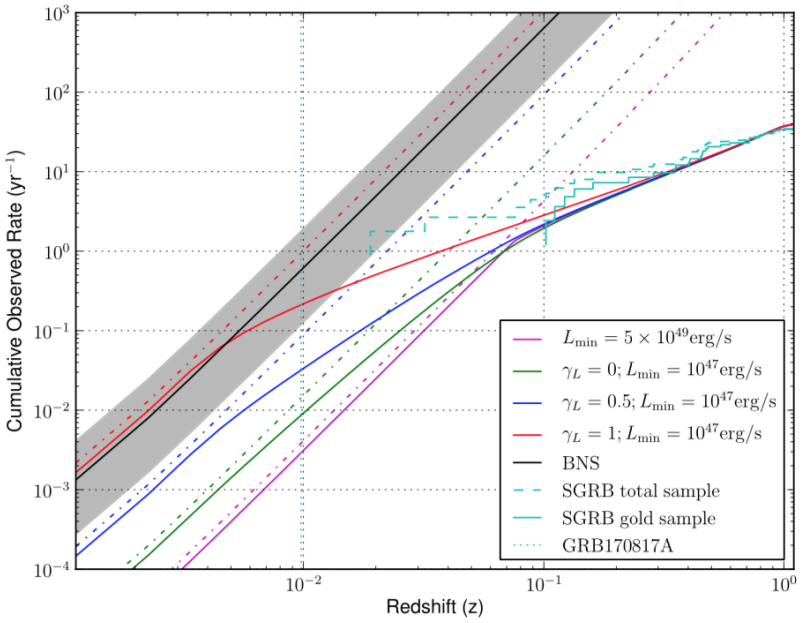

Abbott et al. (2017a),

Binary Neutron Star Mergers

Early: Post-merger Oscillations & GWs

GRAVITATIONAL WAVES

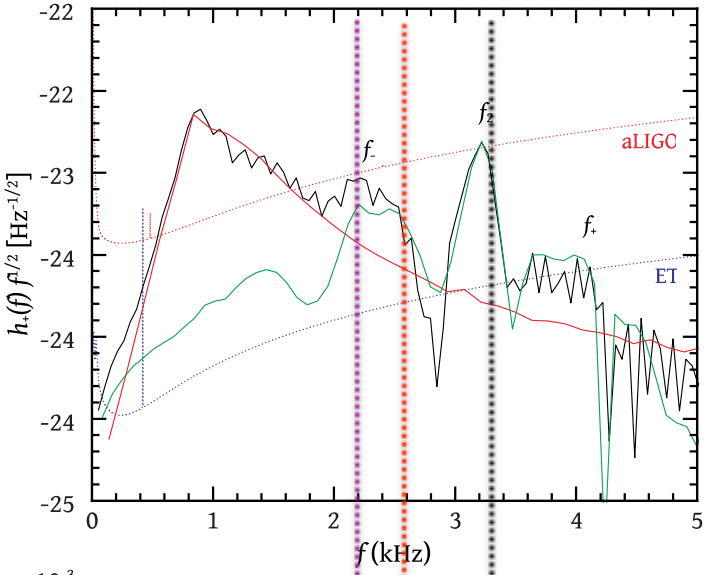

Stergioulas et al. (2011)
Bauswein, Stergioulas (2015)
…
Krüger, Kokkotas (2019)

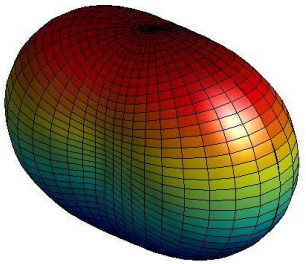

NEUTRON STAR OSCILLATIONS

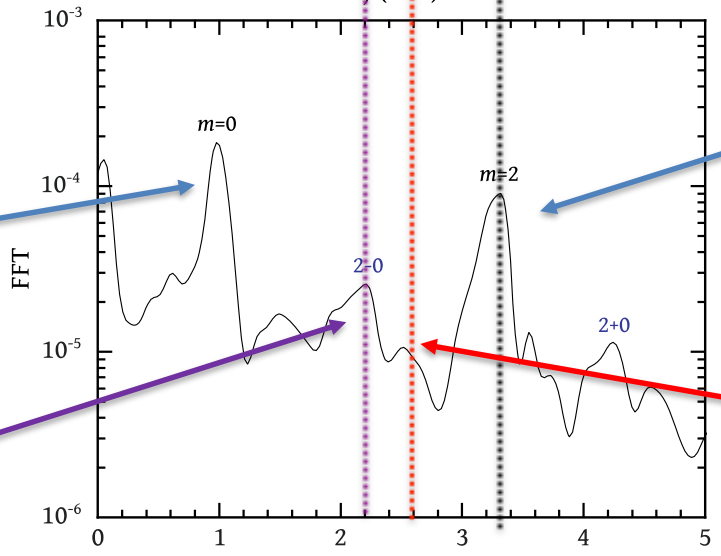

l=m=0 linear quasi-radial mode

Quasi-linear combination frequency (f_{2-0})

l=m=2 linear f-mode (f_{peak})

nonlinear spiral frequency

Binary Neutron Star Mergers
LATE post-merger phase

Formation of a "stable" NS

Slowdown due to three competing mechanisms:

I. Typical dipole B-field spindown

$$t_{sd} \approx 7 \left(\frac{B_d}{10^{15}G}\right)^{-2} \left(\frac{P}{1ms}\right)^{2} hr$$

II. Deformed Magnetar Model

Dall'Osso-Giacomazzo-Perna-Stella 2015

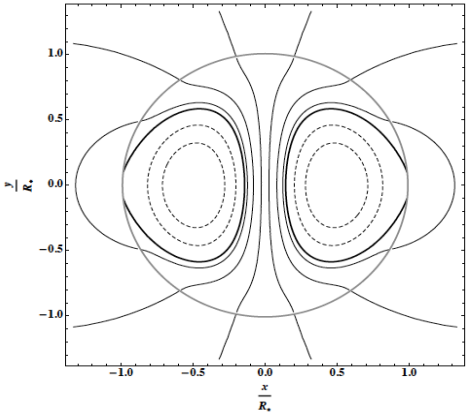

III. Rotational Instabilities

Doneva-Kokkotas-Pnigouras 2015

$$l = 2, m = 2$$

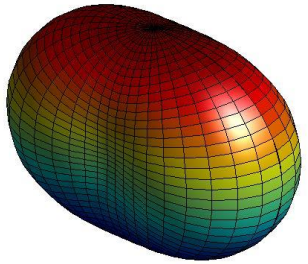

Binary Neutron Star Mergers
Short γ-ray light curves

- The favored progenitor model for SGRBs is the merger of two NSs that triggers an explosion with a burst of collimated γ-rays.
- Following the initial prompt emission, some SGRBs exhibit a plateau phase in their X-ray light curves that indicates additional energy injection from a central engine, believed to be a rapidly rotating, highly magnetized neutron star.
- The collapse of this "protomagnetar" to a black hole is likely to be responsible for a steep decay in X-ray flux observed at the end of the plateau.

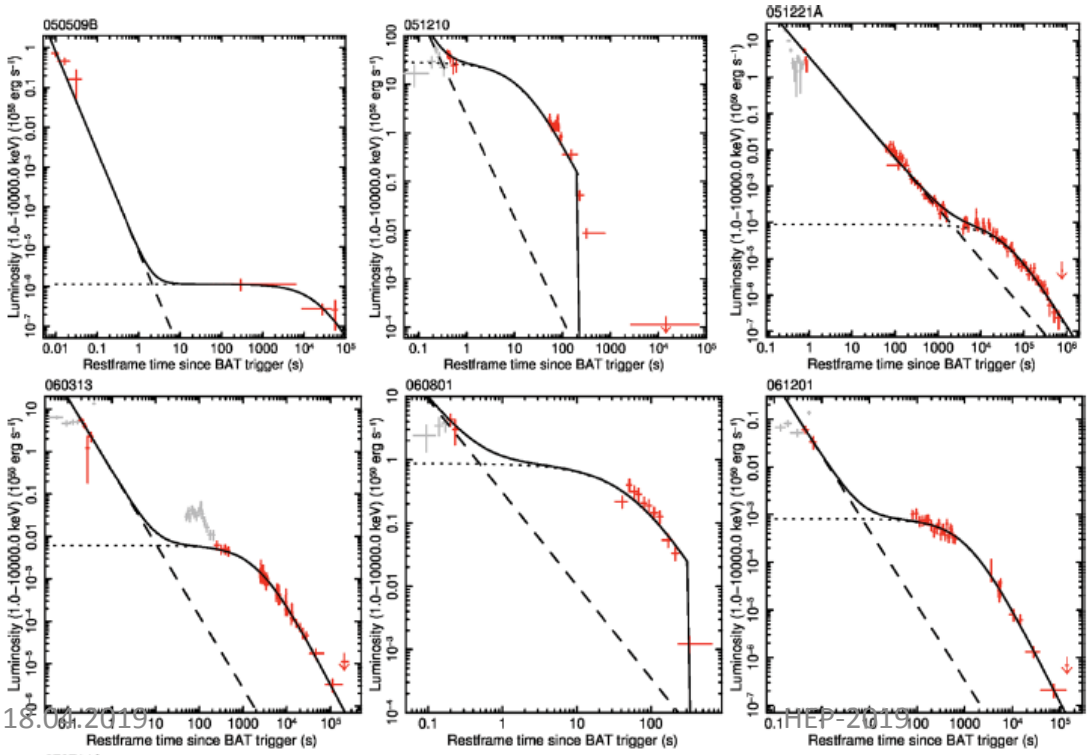

Rowlinson, O'Brien, Metger, Tanvir, Levan 2013

Post-Merger NS:
F-mode instability vs Magnetic field

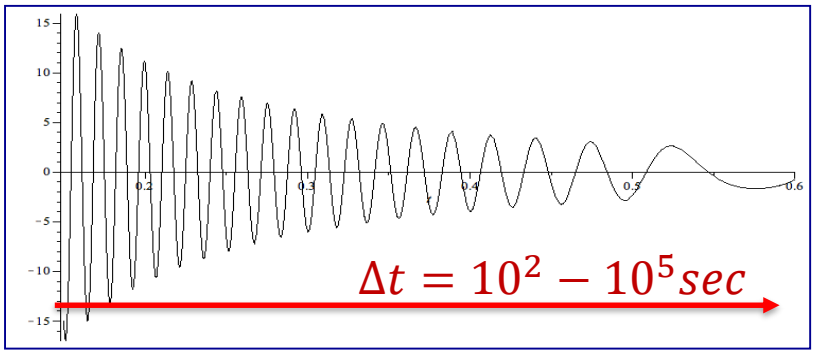

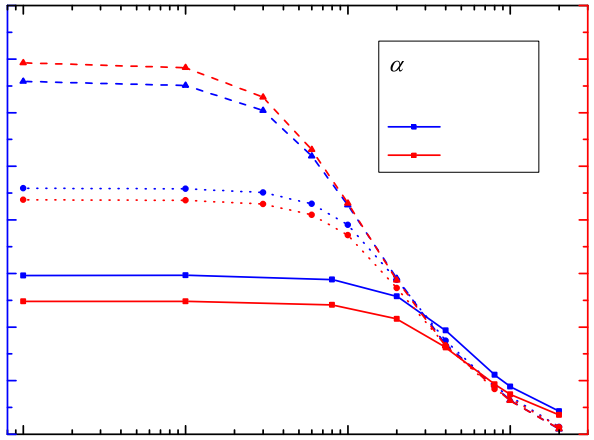

Competition between the B-field and the secular instability

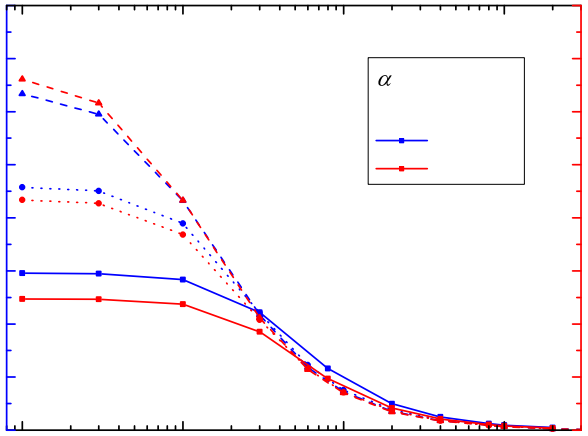

GW frequencies:

WW2a: 920-1000 Hz
APR: 370–810 Hz
WFF2b: 600–780 Hz

Doneva-Kokkotas-Pnigouras 2015

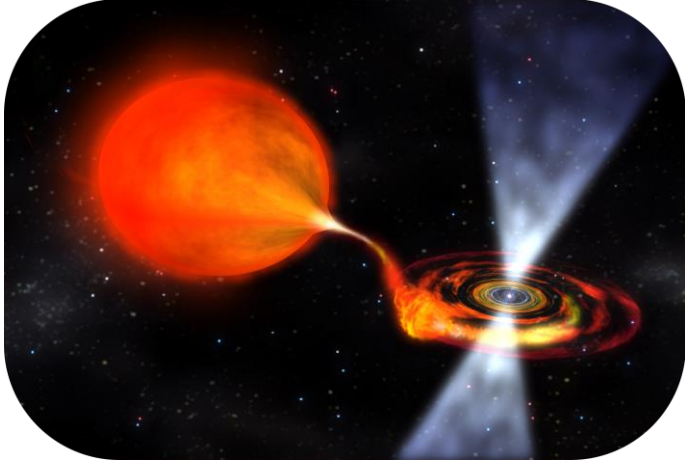

Isolated Neutron Stars as Sources of Continuous

- Haskell, Andersson, D'Angelo, Degenaar, Glampedakis, Ho, Lasky, Melatos, Oppenoorth, Patruno, Priymak (arXiv:1407.8254)
- Kokkotas, Schwenzer EPJA (2016) (arXiv:1510.07051)
- …and references therein

NS as Continuous Sources
r-modes & "mountains"

"Mountains": Deformations that are static (at dynamical timescales) typically in the crust. *The finite shear modulus of the crystalline crust offers the possibility of supporting a deformation* (Bildsten 1998)

- **Strong magnetic fields** can also confine material and lead to deformations that could be quite large (magnetars).
- In LMXBs **accretion process** can lead to material spreading equatorially and compressing the field making it locally strong enough to sustain sizable mountains.

- **Modes of oscillations** can grow to large amplitude and lead to GWs.
- The prime candidate in LMXBs is the **r-mode** (restoring force the Coriolis force).
- Primarily toroidal perturbations and the Eulerian velocity perturbation is:

$$\delta \mathbf{v} = \alpha \left(\frac{r}{R}\right)^{l} R\Omega \mathbf{Y}^{B}_{lm} e^{i\omega t}$$

Observational constraints for ellipticity : $\sim 8.5 \times 10^{-6}$

Abbot at al arXiv:1607.02216

Neutron Stars as Continuous Sources
r-modes

The classical instability window

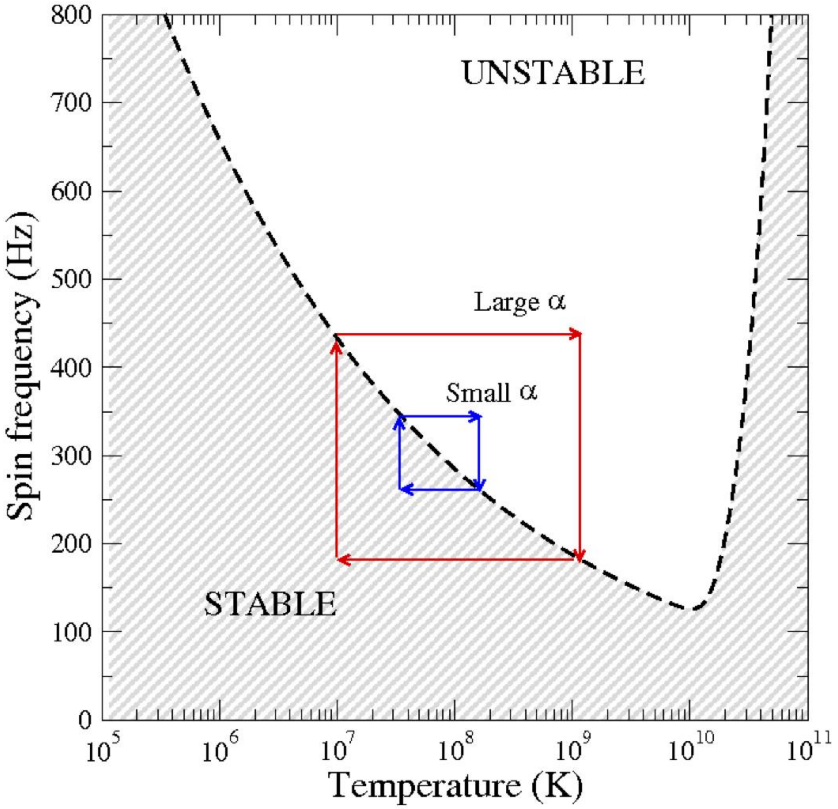

- **Large α**: the system enters into the unstable region with very short duty cycle ~1%.
- **Small α** (~10^{-5}): the duty cycle much longer but the system will never depart from the instability curve.

In both cases it is **highly unlikely** to observe a system in the unstable region

Andersson, Kokkotas, Stergioulas, 1999
Levin Y. 1999
Andersson, Jones, Kokkotas, Stergioulas, 2001
Andersson-Kokkotas 2001
Heyl 2002
…

Saturation of the Instability
Parametric Resonance

$$\dot{Q}_\alpha = \gamma_\alpha Q_\alpha + i\omega_\alpha \mathcal{H}\, Q_\beta Q_\gamma\, e^{-i\Delta\omega t}$$
$$\dot{Q}_\beta = \gamma_\beta Q_\beta + i\omega_\beta \mathcal{H}\, Q^*_\gamma Q_\alpha\, e^{i\Delta\omega t}$$
$$\dot{Q}_\gamma = \gamma_\gamma Q_\gamma + i\omega_\gamma \mathcal{H}\, Q_\alpha Q^*_\beta\, e^{i\Delta\omega t}$$

Detuning $\Delta\omega$

Coupling coefficient $\mathcal{H}$

Growth/damping rates γ_i

$$\text{Detuning } \Delta\omega \equiv \omega_\alpha - \omega_\beta - \omega_\gamma \approx 0$$

resonance condition

Parametric resonance: $\mathcal{H} \neq 0$ and $\Delta\omega \approx 0$

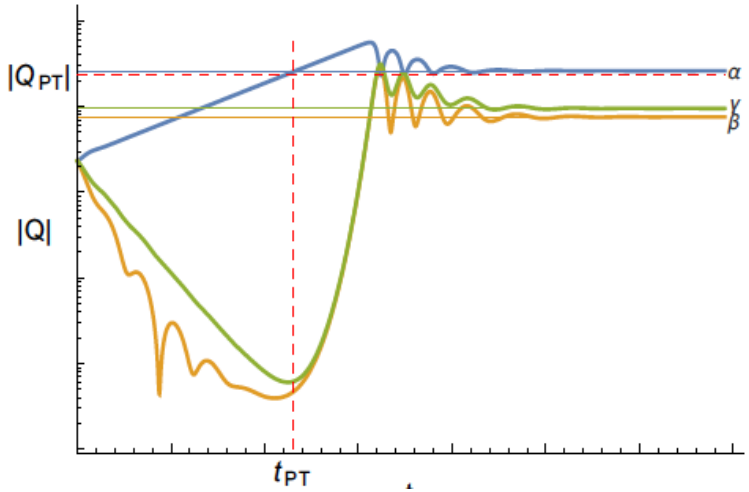

- Parent feeds daughters and makes them grow
- *Parametric threshold:* daughters grow when

$$|Q_\alpha|^2 > |Q_{\rm PT}|^2 \equiv \frac{\gamma_\beta \gamma_\gamma}{\omega_\beta \omega_\gamma \mathcal{H}^2}\left[1 + \left(\frac{\Delta\omega}{\gamma_\beta + \gamma_\gamma}\right)^2\right]$$

- $|Q^{\rm sat}_\alpha| \approx |Q_{\rm PT}|$

Pnigouras, Kokkotas (2015,16)

Neutron Stars as Continuous Sources
r-modes

The classical instability window

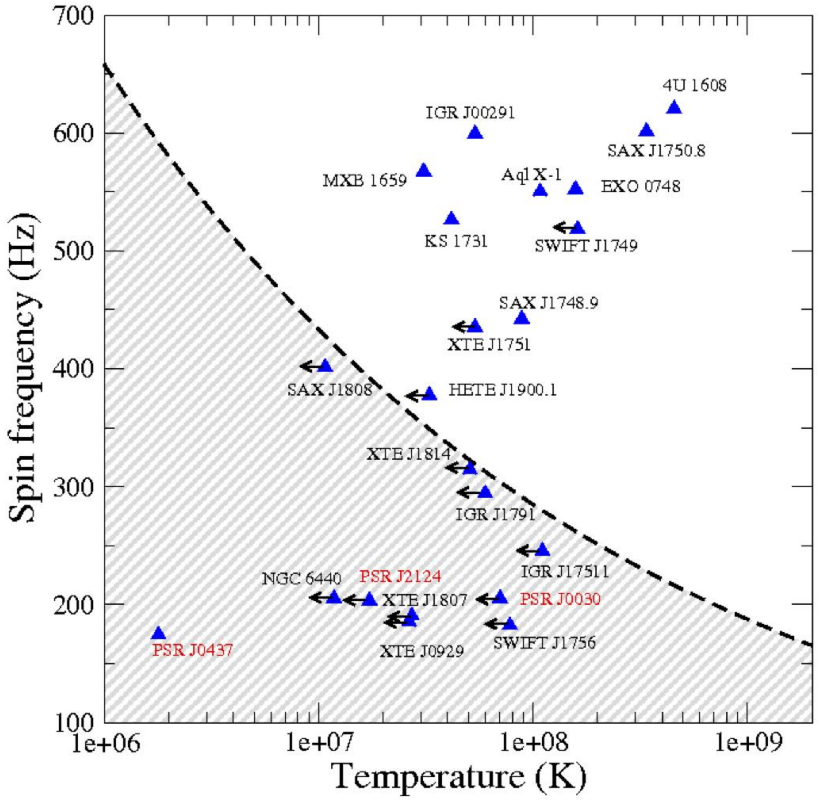

Haskell et al 2012
Mahmoodifar-Strohmayer 2013
Ho et al 2011

Observational data suggest that many systems would sit inside the instability window !!

The "minimal" NS model described earlier is not consistent with observations.

Either

we should include extra sources of damping (hyperons, deconfined quarks, mode coupling, torsional crust oscillations, magnetic braking**, superfluid mutual friction)**

OR

The r-mode amplitude is too **small** that although the NS is indeed unstable does'n affect impact on the thermal and spin evolution.

NS as Continuous Sources
Magnetic Mountains

- **Accretion** does not only lead to thermal perturbations in the crust, but also **perturbs the magnetic field structure.**
- After matter is accreted at the magnetic poles it spreads towards the equator, compressing the field and leading to an overall suppression of the large-scale dipolar structure, but also to local enhancements that can support a sizeable mountain (Melatos et al 2004,2005, 2009,…)
- The mass quadrupole $Q_{22}(\approx 10^{39} - 10^{40} g\ cm^2$ [Haskell et al 2006, Johnson-McDaniel, Owen 2013]) depends on the accreted matter M_a and the critical mass M_c at which the process saturates and both of them (Q_{22} and M_c) on the EOS.

- Predictions [Haskell et al. 2015] for the GW emission from *known LMXBs*, given a magnetic mountain with a background magnetic field of **B = 10^{10} G** or **B = 10^{12} G**.
- Here *the mountain is assumed to* ***be stable in-between outbursts*** *and can thus be built gradually over the life time of the system.*

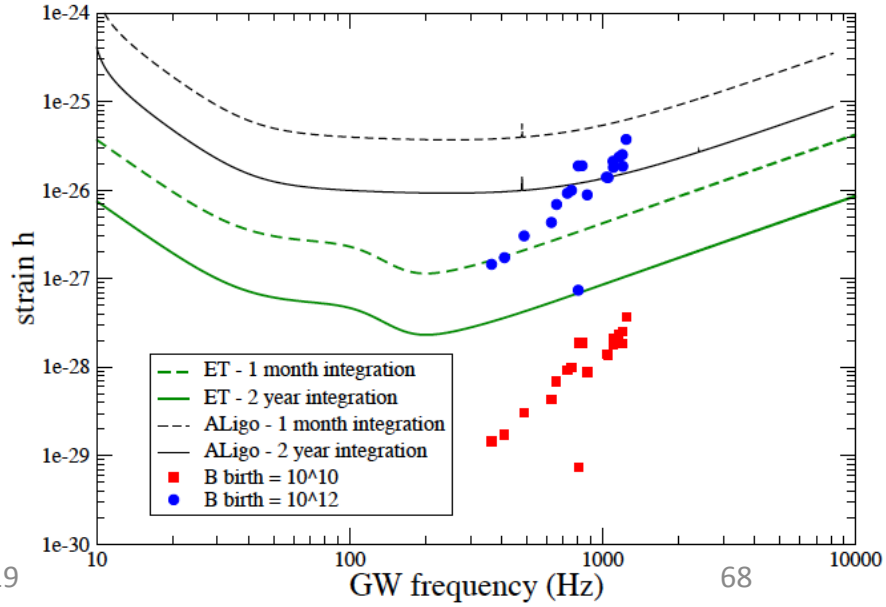

NS as Continuous Sources
Thermal Mountains on NSs

- In the the thermal case the mountain arises as the crust is heated by reactions that occur as accreted material is submerged deep into the crust.
- As it reaches higher densities several pycnonuclear reactions occur, which heat the star locally.
- If part of this heating is asymmetric, and quadrupolar in particular, this can lead to a mass quadrupole

The LIGO and ET sensitivity curves compared to the GW amplitude for persistent LMXBs (Haskell et al 2015)

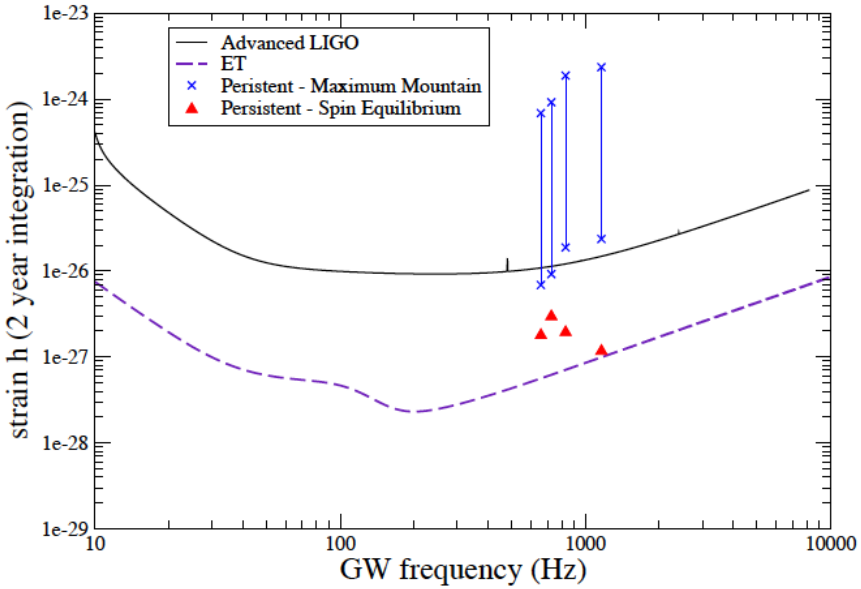

- Here was assumed the **maximum deformation** that the crust can sustain
- The error bars account for **uncertainties** in mass and EOS.
- For comparison it is shown the GW amplitude that would be needed for torque balance.

- No cyclotron lines have been detected
- The magnetic fields are much weaker ~10^8G

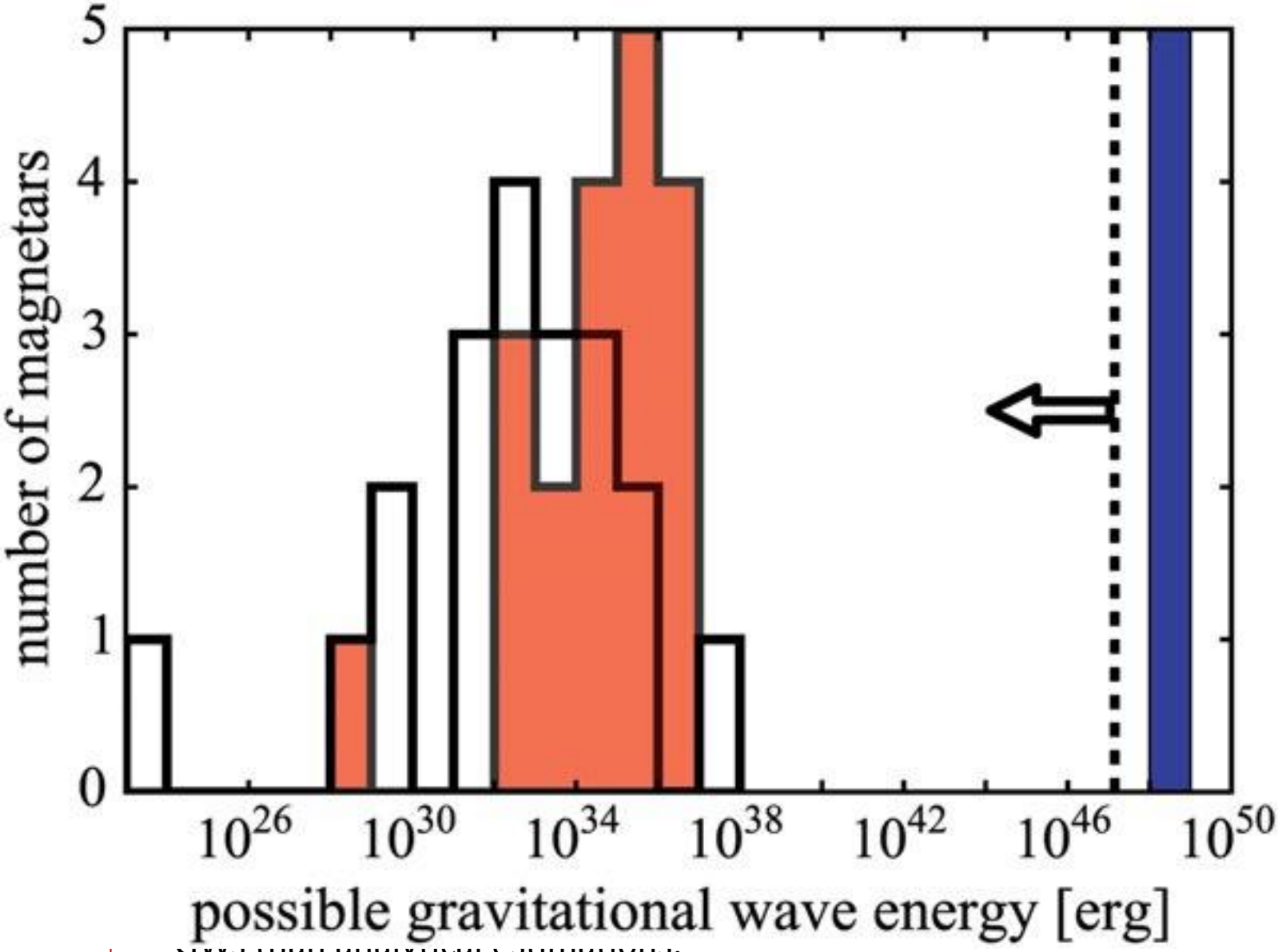

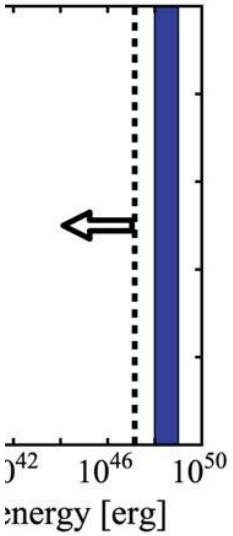

they both
itted in

- Actually, early-LIGO analysis set an upper limit for the energy emitted in GWs (dashed line) i.e. **$E_{GW} < 10^{46}$ erg**

NS as Continuous Sources
Latest LIGO results

Amplitude of the signal

$$h_0 = \frac{4\pi^2 G}{c^4}\frac{I_{zz}\epsilon f^2}{d}$$

Ellipticity

$$\epsilon = \frac{c^4}{4\pi^2 G}\frac{h_0 d}{I_{zz} f^2}$$

Spin-down due only to GWs

$$|\dot{f}| = 1.72\times 10^{-14}\left(\frac{I_{zz}}{10^{38}\,\mathrm{kg\cdot m^2}}\right)\left(\frac{f}{100\,\mathrm{Hz}}\right)^{1/2}\left(\frac{\varepsilon}{10^{-6}}\right)^2\ [\mathrm{Hz/s}].$$

- **Targeted searches** for known pulsars
- **Directed searches** look for signals from known sky locations like : Galactic center, supernovae remnants and LMXBs
- **All sky signals** from unknown sources.

ε	d	df/dt
~10^{-5}	10 kpc	10^{-8} -10^{-9}
~10^{-6}	1 kpc	10^{-10} - 10^{-11}
~10^{-7}	0.1 kpc	10^{-12} – 10^{-13}
~10^{-8}	0.01kpc	10^{-14} -10^{-15}

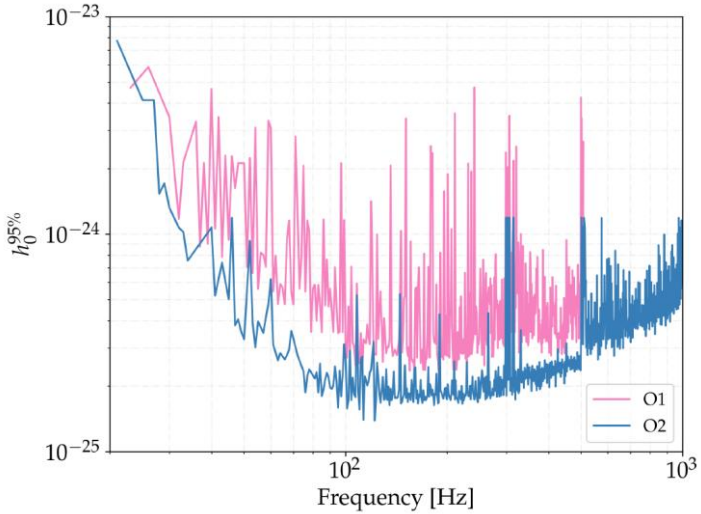

Comparison of O1 and O2 in strain amplitudes:
O1: 20-475 Hz ---- **O2:** 20-1000Hz

What should expect

BLACK-HOLE MERGERS

- Improvement **of the merger rates will** yield a wealth of information — **about how black holes are formed and evolve**,
- **Measuring the individual SPINS will be a major issue:**
  - If the black holes' rotational axes are parallel, that would suggest they have a common origin and started out as two stars orbiting together.
  - Conversely, spins that are randomly aligned imply that the black holes formed separately and then began to orbit each other later on.
- Resolve the **"Echo"** issue
- Further constraints on alternative theories of gravity, exotic objects, …

What should expect

NEUTRON STAR MERGERS

- NS equation of state will be constraint even further
- Mergers *which will not lead directly to black-hole*, will provide unique information of the post-merger evolution, cooling, amplification of magnetic fields, instabilities, r-processes, …
- Important unique information for EM wave astrophysics
- Further constraints on alternative theories of gravity, exotic objects, …

BLACK-HOLE NEUTRON STAR MERGERS

- ALL previous

COLLAPSE

- Quite unlikely
- If it happens will be of unique importance for multi-messenger astrophysics.

ISOLATED SOURCES

- Quite disappointing results up to now
- Possible ellipticities too small

The Future of ATG

After 104 years there is someone STILL smiling at us

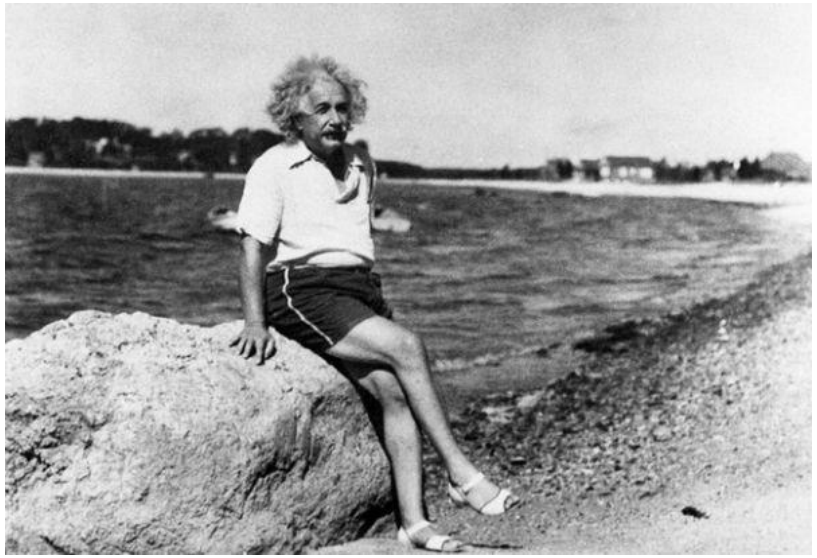

…because GTR still prevails !!

--Many of the branches of the *"Gravity Apple Tree"* have already been cut
--More will follow
--But probably a few may make it till ET, Cosmic Explorer and LISA

Genealogical tree of the gravitation theories developed between 1904 and 2014, structured with the aid of formal concept analysis method, and a diachronic perspective. Authors and dates are